จุฬาลงกรณ์มหาวิทยาลัย

ทุนวิจัย

กองทุนรัชดาภิเษกสมโภช

รายงานผลการวิจัย

การสังเคราะห์ดินเหนียวนาโนที่มีรูพรุนดัดแปรด้วยโครโมฟอร์เพื่อการเตรียมฟิล์มบรรจุภัณฑ์ที่มีความสามารถดูดจับก๊าซเอธิลีนและเป็นตัวตรวจวัดทางแสง

โดย

ผศ. ดร. หทัยกานต์ มนัสปิยะ

กันยายน พ.ศ. 2556

กิตติกรรมประกาศ

งานวิจัยนี้ได้รับทุนอุดหนุนการวิจัยจากกองทุนรัชดาภิเษกสมโภช (Ratchadaphiseksomphot Endowment Fund) และการสนับสนุนบางส่วนจากทุนวิจัยเพื่อพัฒนาเศรษฐกิจและสังคมด้วยวิทยาศาสตร์และเทคโนโลยี จากสำนักงานคณะกรรมการวิจัยแห่งชาติ

ชื่อโครงการวิจัย	การสังเคราะห์ดินเหนียวนาโนที่มีรูพรุนดัดแปรด้วยโครโมฟอร์เพื่อการเตรียมฟิล์มบรรจุภัณฑ์ที่มีความสามารถดูดจับก๊าซเอธิลีน และเป็นตัวตรวจวัดทางแสง
ชื่อผู้วิจัย	ผศ.ดร. หทัยกานต์ มนัสปิยะ รศ.ดร. รัตนวรรณ มกรพันธุ์ นางสาวสุภัจฉรี บุญเรือง
เดือนและปีที่ทำวิจัยเสร็จ	กันยายน 2556

บทคัดย่อ

บรรจุภัณฑ์ฉลาดสำหรับบ่งบอกความสดของผลไม้ที่มีอัตราการหายใจเปลี่ยนแปลงตามอายุ สามารถเตรียมได้โดยใช้พอลิเอทิลีนความหนาแน่นต่ำร่วมกับแร่ดินเหนียวโครงสร้างรูพรุนที่ดัดแปรด้วยโบรโมไทมอลบลูนาโนคอมพอสิต วัสดุรูพรุนดัดแปรด้วยโครโมฟอร์สามารถตรวจวิเคราะห์ด้วยเทคนิคการดูดซับ-ปลดปล่อยไนโตรเจน เทคนิคเอ็กซ์เรย์ดิฟแฟรกชัน และกล้องจุลทรรศน์อิเล็กตรอนแบบส่องกราด วัสดุนาโนคอมพอสิตที่ไวต่อการเปลี่ยนแปลงความเป็นกรด-เบสสามารถเตรียมได้โดยใช้เครื่องอัดรีดแบบเกลียวคู่ และขึ้นรูปเป็นแผ่นฟิล์มโดยใช้เครื่องขึ้นรูปแบบอัด ฟิล์มพอลิเอทิลีนความหนาแน่นต่ำนาโนคอมพอสิตถูกนำมาประยุกต์ใช้ในการบอกความสดของผลไม้ที่มีอัตราการหายใจเปลี่ยนแปลงตามอายุ เนื่องจากสีของโบรโมไทมอลบลูในนาโนคอมพอสิตฟิล์มจะเปลี่ยนจากสีเขียวเป็นเหลือง เมื่อสัมผัสกับก๊าซคาร์บอนไดออกไซด์และน้ำ ซึ่งสามารถนำไปเปรียบเทียบได้กับการหายใจของผลไม้ที่มีอัตราการหายใจเปลี่ยนแปลงตามอายุ และมีผลทำให้ค่าความเป็นกรด-เบสลดลง ดังนั้นฟิล์มนาโนคอมพอสิตอินดิเคเตอร์จึงสามารถใช้เป็นวัสดุที่ไวต่อการเปลี่ยนแปลงความเป็นกรด-เบส รวมทั้งสามารถยืดอายุการเก็บรักษาเพื่อใช้ในบรรจุภัณฑ์ได้อย่างมีประสิทธิภาพอีกด้วย

Project Title	Synthesis of Chromophores Modified Porous Clay Heterostructure for Preparing Ethylene Scavenger and Optical Sensor Packaging Film
Name of the Investigators	Asst. Prof. Hathaikarn Manuspiya Assoc. Prof. Rathanawan Magaraphan Supatcharee Boonruang
Year	September 2013

Abstract

Smart packagings for detecting climacteric fruit freshness were prepared based on low density polyethylene (LDPE)/chromophores (bromothymol blue) modified PCH (PCH-BTB) nanocomposite films. The incorporation of chromophores in porous materials was investigated by N_2 adsorption-desorption, XRD and SEM. The nanaocomposite was prepared by twin screw extruder and fabricated into nanocomposite film by compression molding. The color change of LDPE/PCH-BTB nanocomposite films from green to yellow correlated with standard CO_2 levels, which can be compared to CO_2 levels from respiration during fruit ripening. Porous clay improved the barrier properties of nanocomposite indicated by the reduction of oxygen transmission rate. Thus, LDPE/PCH-BTB nanocomposite films can be applied for detecting the quality of climacteric fruit by color change. In addition, this pH indicator can prolong the shelf-life of product by incorporated porous materials into the films.

TABLE OF CONTENTS

LIST OF TABLES

LIST OF FIGURES

FIGURE **PAGE**

CHAPTER IV

FIGURE **PAGE**

1. INTRODUCTION

Nowadays food packaging systems are increasingly important in food products because the problem of post harvest fruits and vegetables or meat products are the limitation of their fresh and shelf-life. Innovative packaging with enhanced functions is developing to response the consumer demands or industrial production in order to preserve the fresh and tasty of convenient food products by prolonged shelf-life and controlled quality.

In general, innovative packaging for food product can be categorized into sub-different class; active and intelligent packaging. Active packaging is defined as a packaging that changes the condition of the packed food to extend shelf-life or to improve safety or sensory properties while maintain the quality of packaged food. Intelligent packaging, distinctly different concept from active packaging system, it is the packaging that monitor the condition of packaged food to give information about the quality of food during transport and storage to the manufacturer, retailer and consumer.

Up to the present time, intelligent packaging technologies are used for quality control such as time-temperature indicators, integrity indicators (leak indicators) and freshness indicators. At present, freshness indicators are interesting techniques which are used to monitor the status of food spoilage. Freshness indicators provide the direct product quality information resulting from microbial growth or chemical changes within food product resulting in pH changes, formation of toxic compounds, off-odors and gas formation. The indication of freshness can be based on the reaction between the indicator and the metabolites produced from food product.

Recently, porous clay heterostructure (PCH), one of the most common used materials in smart packaging due to the excellent barrier properties as well as superior ability of gas adsorption from its high surface area. Moreover, in order to synthesize PCH with organic-inorganic hybrid structure, the structure of inorganic frame works is combined with organic group in pore structure for providing the high gas adsorption property for gas molecules and selectivity for organic compound.

The food industries are interested in developing methods to evaluate the real time freshness of food product. The development of a freshness color indicator in the form of smart packaging is the one concept that cans response the industry demand.

In this study, we have focused on the preparation of colorimetric indicator for detecting climacteric fruit freshness based on low density polyethylene/ chromophores (bromothymol blue) modified PCH nanocomposite films. Bromothymol blue acted as the pH indicators for determine freshness of product through the visible color change. The mechanical properties, thermal properties, permeability and the effect of processing conditions of the nanocomposites were investigated. In addition, leaching of the dye was also studied to assess the suitability of the sensor formulation for food packaging application.

2. LITERATURE REVIEW

2.1 Intelligent Packaging

Intelligent packaging is defined as a packaging system that monitors the condition of packaged food to give information about the quality of the packaged food during transport and storage (Ahvenainen R., 2003).

Intelligent packaging is defined as a packaging system that is capable of carrying out intelligent functions (such as detecting, sensing, recording, tracing, communicating, and applying scientific logic) to facilitate decision making to extend shelf life, enhance safety, improve quality, provide information, and warn about possible problems (Yam L. K. *et al.*, 2005).

Many intelligent packaging concepts which are used to determine the quality of packaged food involve external indicator i.e. indicators which are attached outside the package (time temperature indicator) and internal indicators which were placed inside the package, either to the head-space of the package or attached into the lid (oxygen indicators, carbon dioxide indicators, microbial growth indicators and pathogen indicators).

Table 2.1 Examples of external and internal indicators and their working principle or reacting compounds to be used in intelligent packaging for quality control of packed food (Ahvenainen R. *et al.*, 2003)

Indicator	Principle/reagents	Give information about	Application
Time-temperature indicators (external)	Mechanical Chemical Enzymatic	Storage condition	Foods stored under chilled and frozen conditions
Oxygen indicators (internal)	Redox dyes pH dyes Enzymes	Storage condition Package leak	Food stored in packages with reduced oxygen concentration
Carbon dioxide indicator (internal)	Chemical	Storage condition Package leak	Modified/controlled atmosphere food packaging

Indicator	Principle/reagents	Give information about	Application
Microbial growth indicators (internal/external) i.e. freshness indicators	pH dyes All dyes reacting with certain metabolites (volatiles or non-volatiles)	Microbial quality of food (i.e. spoilage)	Perishable foods such as meat, fish and poultry
Pathogen indicators (internal)	Various chemical, immunochemical methods reacting with toxins	Specific pathogenic bacteria such as Escherichia coli O157	Perishable foods such as meat, fish and poultry

2.2 Freshness Indicator

Freshness indicators are used to indicate the product quality information resulting from microbial growth or chemical changes within a food product during storage and transportation. One of concepts for freshness indicator are presented based on indicators sensitive to pH change, which change color in the presence of volatile compounds produced during spoilage. The indicator exhibits the irreversible change in visual appearance due to microbial growth during food deterioration inducing pH change. Volatile nitrogen compound, carbon dioxide, hydrogen sulphide and organic acid are proposed to be suitable target molecules for pH-sensitive indicators.

For example, Hong *et al.* (2000) studied the use of color indicators as a packaging system for evaluating kimchi fermentation. The color indicating films consisted of polypropylene (PP) resin, calcium hydroxide as a CO_2 absorbent and bromocresol purple (BP) or methyl red (MR) as a chemical dye. Kimchi fermentation was assessed for titratable acidity (TA) and color changes of the indicators were measured and expressed as Hunter values as well as total color difference (TCD). From the color data, TCD values of bromocresol purple (BP) type indicator ranged 27±33 and were much more than those of methyl red (MR) type. In the case of BP, Hunter L and b values increased gradually with storage time while Hunter a value decreased slowly and then remained constant. However, Hunter L and b values of the

indicator containing MR decreased exponentially while Hunter a value increased remarkably and remained constant. The result means that color of the BP type indicator turned from initially blue to finally light green, and that of the MR type turned from light orange to red. The rate of color changes was different depending on temperature but with the same pattern. Moreover, TCD of each indicator closely correlated with TA, as little influenced by temperature. The TA values give a nearly straight line against the TCD values of the BP type indicator, whereas they formed a concave curve over those of the MR type. Present result suggests that the BP type indicator can be used successfully as a full time-fermentation indicator for kimchi products. However, the MR type may be applied only as a ripeness/unripeness indicator to packaged kimchi because its color change rate nearly reaches to zero at the TA values more than 0.7 mg/dl.

Tassanawat *et al.* (2007) prepared pH-sensitive modified clay and polypropylene nanocomposites for smart packaging to represent the degree of deterioration of fresh milk. Milk deterioration was assessed for titratable acidity (TA) and color change of the bromothymol blue (BMB) as an indicator was measured by total color difference (TCD) value. The result of TA and TCD values suggested that BMB can be used as fresh milk deterioration indicator. The nanoćlay composites incorporating pH indicator were melt compounding through a twin screw extruder using surlyn® as a reactive compatibilizer. Subsequently, the nanoclay composites were fabricated into the sample sheet for pH-sensitive test.

Nopwinyuwong *et al.* (2010) prepared a colorimetric mixed pH dye-based indicator for the development of intelligent packaging as a chemical barcode for real-time monitoring of intermediate-moisture dessert spoilage. The on-package indicator contains mixed pH-sensitive dyes, bromothymol blue and methyl red, that respond through visible color change to CO_2 as a spoilage metabolite. The result of the change in CO_2 level monitored by the indicator label in golden drop at 25 and 10°C showed that a clear spectrum from bright light green to orange-red corresponded with exposed CO_2 during storage time. The minimal spoilage level of golden drop occurred on days 6 and 28 during storage at 25 and 10°C respectively as shown in Figure 2.1.

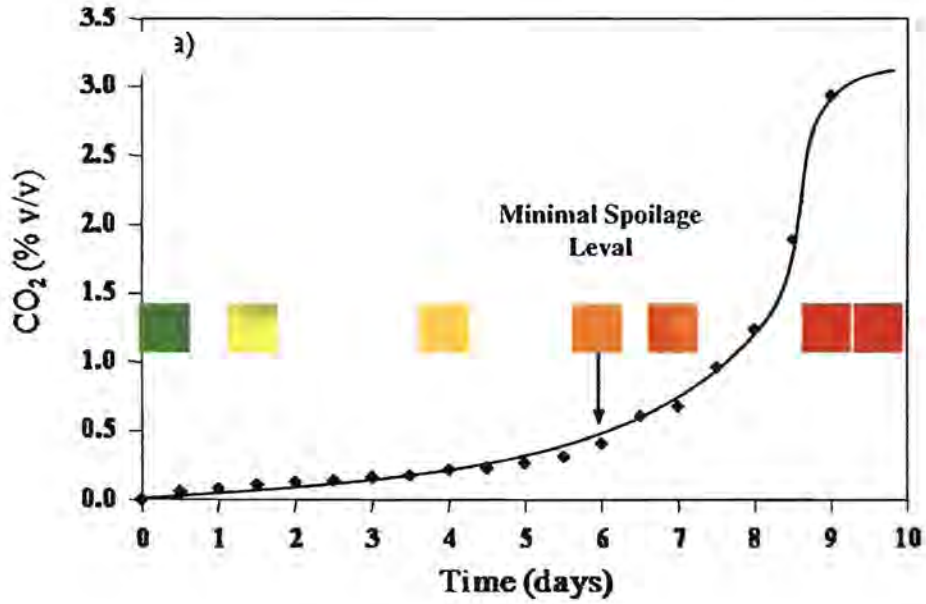

Figure 2.1 Change in CO_2 level in golden drop at 25°C with indicator level which showed color change with time.

2.3 Climacteric Fruit Freshness

Generally, fruits can be classified as climacteric and non-climacteric. Climacteric is defined as a period in the ontogeny of certain fruits, during which a series of biochemical changes is initiated by the autocatalytic production of ethylene, marking the change from growth to senescence and involving an increase in respiration and leading to ripening. The ripening of climacteric fruit associates with increasing in respiration and ethylene production. The respiration rate will rise up to the climacteric peak and then decline. The majority of fruits that show the climacteric pattern are the apple, apricot, avocado, banana, cherimoya, cantaloupe melon, mango, papaya, passion fruit, pawpaw, peach, pear, plum and tomato.

The climacteric patterns are different in each fruit. For example, the respiration rise of apple and tomato occurs both in fruit detached from and attached to the vine while the avocado only shows a climacteric rise in respiration after detachment from the tree. In many types of tropical and sub-tropical fruits, the rise in

respiration is rapid and the stage of eating ripeness corresponds closely with the climacteric peak in fruits such as avocado, banana, cherimoya and mango. This differs from the apple and tomato which ripening is not complete until after the climacteric peak. Thus in tropical fruits, the various changes involve in the climacteric and ripening show a more complete overlap in time. Moreover, the patterns of respiration and ripening behavior vary among the varieties, the climacteric conditions and the local places.

Respiration can be described as the oxidative breakdown of the more complex materials normally present in cell, such as starch, sugars and organic acids, into simple molecules, such as carbon dioxide and water, with the concurrent production of energy and other molecules that can be used by the cell for synthesis reaction.

The respiration process can be divided into two types, aerobic respiration and anaerobic respiration. Aerobic respiration is a complicated process that involves the enzymatic reaction taking place through the metabolic pathways of glycolysis, the tricarboxylic acid (TCA) cycle, and the association electron transport system. However, the overall reaction describing the respiration process may be simply expressed as

$$C_6H_{12}O_6 + 6O_2 \longrightarrow 6CO_2 + 6H_2O + \text{energy} \qquad (1)$$

Anaerobic respiration, which is sometimes called fermentation, involves the incomplete oxidation of compounds in the absence of O_2 and the accumulation of ethanol, acetaldehyde and CO_2. The respiratory quotient (RQ) is the ratio of CO_2 produced to O_2 consumed during respiration. This is used to identify the type of respiration process. Values of RQ range from 0.7-1.3 for aerobic respiration, depending on the substance being oxidized for carbohydrates, RQ = 1; for lipids RQ < 1; for organic acid RQ> 1. Respiration rate is a good indicator of the likely storage life of horticultural products. The storage life of produces is proportional to the respiration rate a horticultural commodity with a low respiration rate has a longer storage life. For example: apples, citrus fruit, grapes and kiwi fruit. By contrast, high

respiration rate commodities such as strawberry, blackberry, raspberry, avocado and mango have a much shorter storage life (Jirapattarasakul, 2002).

Gane *et al.* (1936) studied the respiration of banana. The respiration of bananas has been measured with fruit of various stages of ripeness under a variety of experimental conditions. First, the respiratory activity in the preclimacteric phase of green and unripe bananas at different temperature was studied. The mean values of the rate of respiration as a function of temperature are shown in Table 2.2. During this time the rate of respiration remains almost steady except at 31°C. The rate of production of carbon dioxide in the preclimacteric phase decreased with time and at this temperature one might expect the onset of a time factor.

Table 2.2 Rate of respiration of green bananas at different temperatures

Temperature (°C)	0	5	12.5	15	20	31
Rate of Respiration (mg/kg/hr)	7.1	10.0	18.5	23.6	35.8	61

Then, the ripening process at different temperature was studied. The characteristic form of the curve of respiratory activity during the ripening process at different temperatures was shown in Figure 2.2. Although the preclimacteric value is practically constant at any temperature, the peak value is not so constant. The effect of temperature on the ripening process as distinct from the time required for ripening to commence can be illustrated by comparing the time taken for the respiration to rise from the pre-ripening phase to the peak value and the times were shown in Table 2.3. Moreover, it was found that the change of color from green to yellow begins to be visible at the peak of respiratory activity, so that fruit may appear to be green and unripe and yet be well advanced on the climacteric. Banana showed the downward drift does not continue after the peak and there was a period when the rate was almost steady. This was followed by a period when it roses again. These changes in the rate of output of carbon dioxide coincided with the changes in the eating quality of the fruit. Just before the respiration has become steady, the fruit has developed its

full yellow color and the eating quality is at its optimum. From this stage onwards the flavor increased in intensity until finally, at the fully ripe stage, it was too pronounced to be palatable. The relation of these stages to the course of respiration at 15° C was shown in Figure 2.4 where *FYC* refers to the full-yellow-color stage and *FR* to the fully ripe stage.

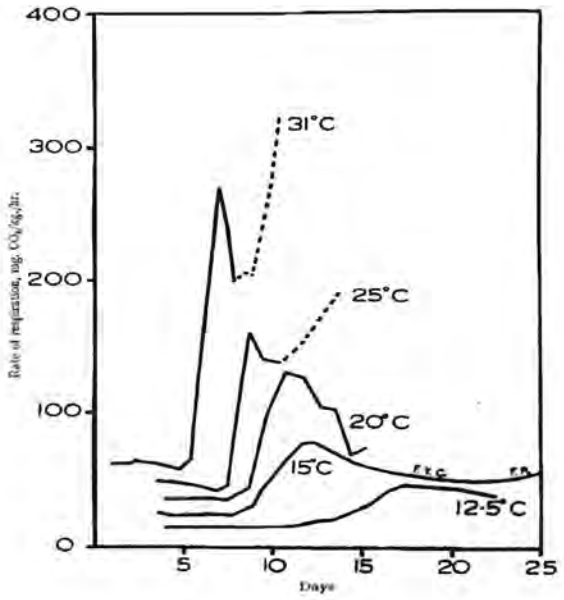

Figure 2.2 Rate of production of carbon dioxide by bananas (initially unripe) at different temperatures.

Table 2.3 The times of respiration rise from pre-ripening phase to peak value at different temperature

Temperature (°C)	12.5	15	20	25	31
Time (Days)	6	4	3.2	1.5	1.5

Dit-u-dompo (1999) studied the mathematical modeling to predict heat generation during banana (Kluai Hom Thong) respiration. Heat generated from the respiration processes was determined at various temperatures and storage gas compositions (O_2 and CO_2). It was essential to know the amount of heat generated

during respiration process of the stored fruit in order to design and optimization an energy-save refrigeration system for stored fruit. In the experiment, heats of respiration and respiration rate of bananas which stored at 13, 17, 20, and 30 °C in ambient air and CAs containing 4% O_2 - 5% CO_2 and 4% O_2 - 10% CO_2 were calculated. The result showed that the obtained model described the rate of heat produced by the respiration processes of banana and the respiration rate as functions of the storage temperature and O_2 and CO_2 concentrations as shown Figure 2.3, 2.4 and 2.5 respectively. The results showed that the heat of respiration and respiration rate increased as the storage temperature increased. At a given storage temperature, the heat of respiration of bananas stored in ambient air was higher than that stored in CAs containing 4% O_2 - 5% CO_2 and 4% O_2 - 10% CO_2, respectively. Moreover, the models were used in calculating the rates of heat produced by bananas stored under a controlled atmosphere (CA) condition at various storage temperatures. The results showed good agreements between the predicted and observed values. Therefore, the models could be used for determining the rate of heat released from bananas stored in a CA storage room.

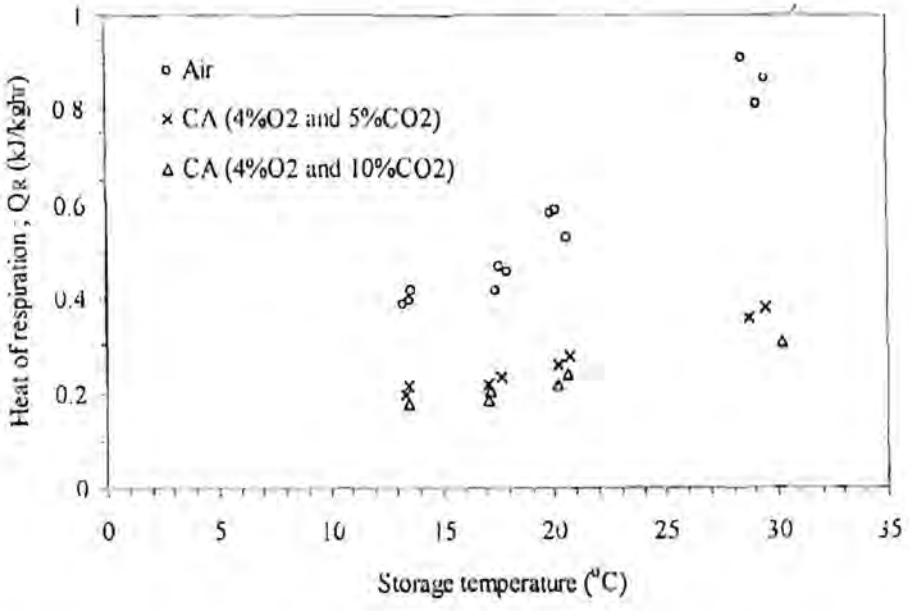

Figure 2.3 Heats of respiration of bananas which stored at 13, 17, 20 and 30 °C in ambient air and CAs containing 4% O_2 - 5% CO_2 and 4% O_2 - 10% CO_2.

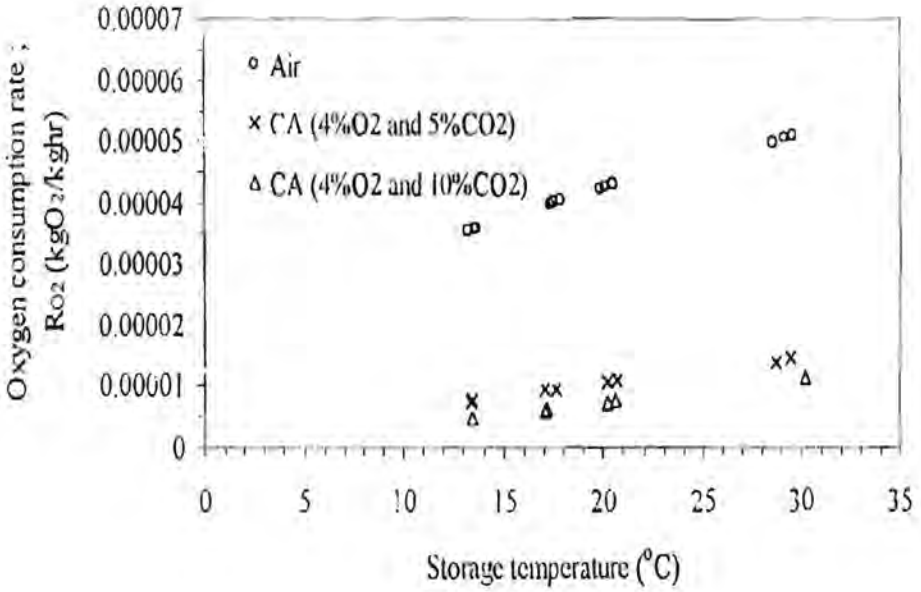

Figure 2.4 O_2 consumption rate of bananas which stored at 13, 17, 20 and 30 °C in ambient air and CAs containing 4% O_2 - 5% CO_2 and 4% O_2 - 10% CO_2.

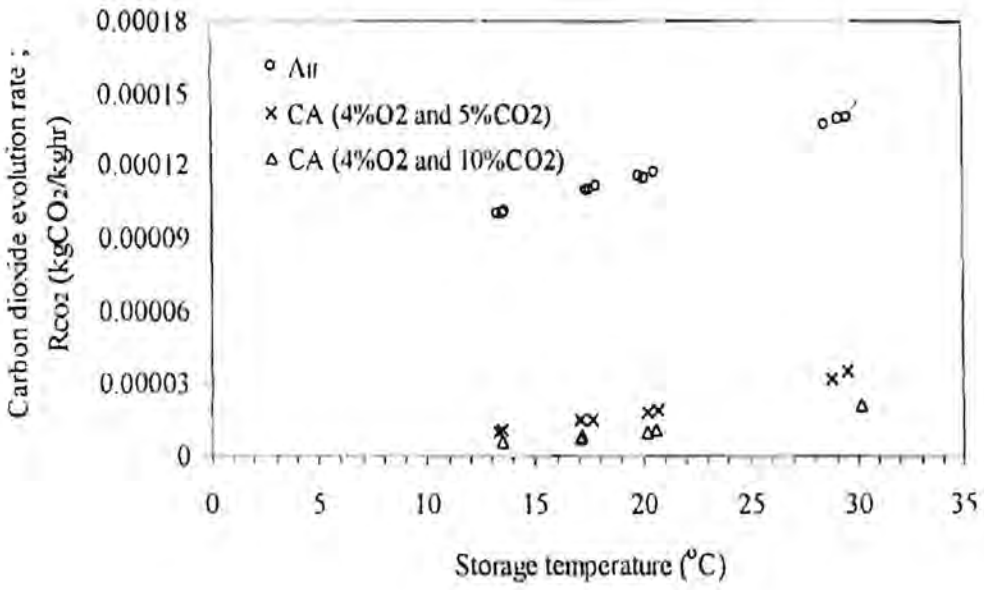

Figure 2.5 CO_2 evolution rate of bananas which stored at 13, 17, 20 and 30 °C in ambient air and CAs containing 4% O_2 - 5% CO_2 and 4% O_2 - 10% CO_2.

Jirapattarasakul (2002) studied heat treatment and respiration model of Mango (Nam Dok Mai). The result showed that respiration kinetic parameters of mango after heat treatments tended to decrease with the increases of heat treatment temperature and the duration time as shown in Figure 2.6. Thus, heat treatment at suitable temperature and duration time could play a role in decreasing respiration rate of mango after heat treatment. The effect of heat treatments on fruit qualities was found that heat treatments at 42°C for 85 min and 46°C for 75 minutes could also reduce weight loss percentage, retard the fruit softening, and increase the color development of mango during storage under MAP at 13°C. Besides, combination between heat treatment and MAP could prolong storage life to 45 days which is 10 days longer than that of fruit without heat treatments. Therefore, appropriate heat treatment could extend the storage time of mango kept under MAP condition.

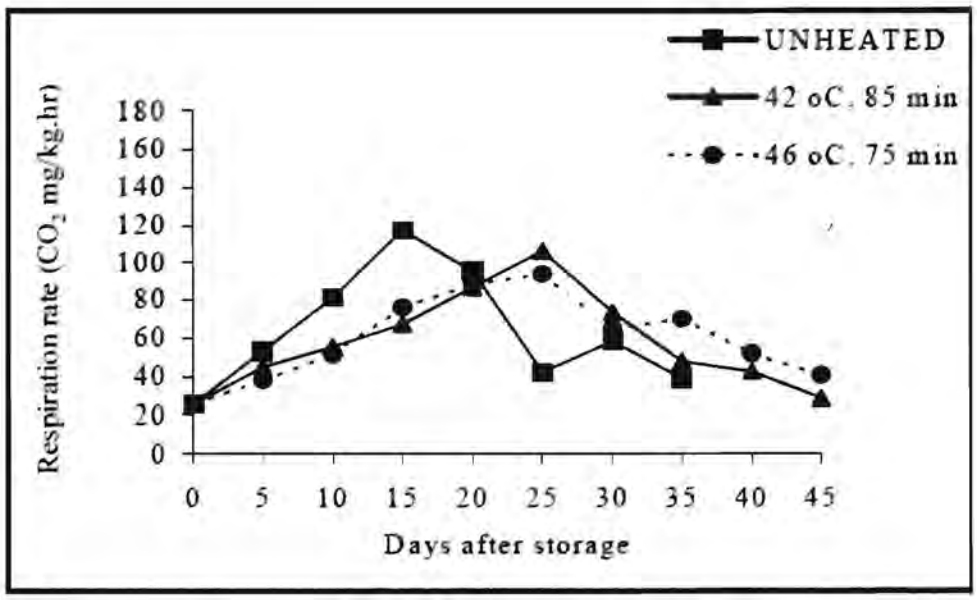

Figure 2.6 Respiration rate of unheated mango, heat treatment at 42 and 46°C for 85 and 75 min, respectively stored at 13°C.

2.4 pH Indicator

The pH indicator is the halochromic chemical compound or the compound which changes color when pH changes occur. The pH indicator can be added in small amounts to a solution so that the pH (acidity or basicity) of the solution can be determined visually. The general reaction scheme of a pH indicator can be formulated as follow equation.

$$HIn + H_2O \rightleftharpoons H_3O^+ + In^- \qquad (2)$$

2.4.1 Bromothymol Blue

Bromothymol blue is a chemical indicator for weak acids and bases which is yellow at pH below 6.0 and blue at pH above 7.6. The pKa for bromothymol blue is 7.10. The chemical is also used for observing photosynthetic activities or respiratory indicators. It will turns from blue to yellow when CO_2 is added. The mechanism of bromothymol blue in acid and basis form is shown in Figure 2.7.

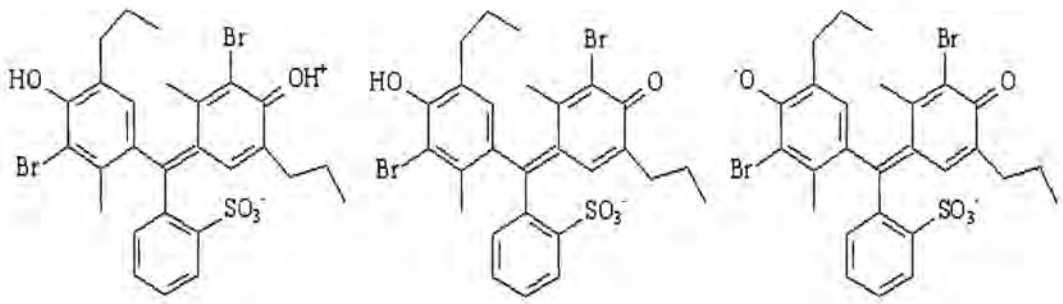

Figure 2.7 Mechanism of bromoyhymol blue indicator in yellow color (left), intermediate between yellow and blue (middle) and blue color (right).

2.5 Structure of Layer Silicate

In the synthesis of nanocomposites, layer silicates are natural or synthetic minerals. They consist of very thin layers that are usually bound together with counter-ions. Their basic building blocks are tetrahedral sheets and octahedral sheets. Tetrahedral sheets compose of silicon which surrounded by four oxygen atoms and octahedral sheets compose of a metal like aluminum which surrounded by six oxygen atoms. Therefore, tetrahedral sheet is fused with an octahedral sheet in 1:1 layered structures (e.g. in kaolinite), whereby the oxygen atoms are shared. On the other hand, the crystal lattice of 2:1 layered silicates or 2:1 phyllosilicates (e.g. in montmorillonite, hectorite and saponite) consists of two-dimensional layers where a central octahedral sheet of alumina is fused to two external silica tetrahedral by the tip, so that the oxygen ions of the octahedral sheet also belong to the tetrahedral sheets, as shown in Figure 2.8. The layer thickness is around 1 nm and the lateral dimensions may vary from 300A° to several microns depending on the particulate silicate (Pavlidou S. and Papaspyrides C., 2008). These layers stack with a regular electrostatic force in between them called the interlayer or the gallery. Isomorphic substitution within the layer (for example, Al^{3+} replaced by Mg^{2+} or by Fe^{2+} in montmorillonite, or Mg^{2+} replaced by Li^{+} in hectorite) generates negative charges. The imbalance of the surface negative charges is compensated by exchangeable cations (typically Na^{+} and Ca^{2+}). The parallel layers are linked together by weak electrostatic forces. As the forces that hold the layer together are relatively weak, the intercalation between the layers is easy. These layers stack with a regular electrostatic force in between them called the interlayer or the gallery. Isomorphic substitution within the layer (for example, Al^{3+} replaced by Mg^{2+} or by Fe^{2+} in montmorillonite, or Mg^{2+} replaced by Li^{+} in hectorite) generates negative charges. The imbalance of the surface negative charges is compensated by exchangeable cations (typically Na^{+} and Ca^{2+}). The parallel layers are linked together by weak electrostatic forces. As the forces that hold the layer together are relatively weak, the intercalation between the layers is easy.

This type of clay is characterized by a moderate negative surface charge (known as the cation exchange capacity, CEC and expressd in mequiv/100g) which

is an important factor to define the equilibrium layer spacing. The charge of the layer is not locally constant as it varies from layer to layer and must rather be considered as an average value over the whole crystal. When the hydrated cations are ion-exchanged with organic cations such as more bulky alkylammoniums, it usually results in a larger interlayer spacing (Pavlidou, 2008).

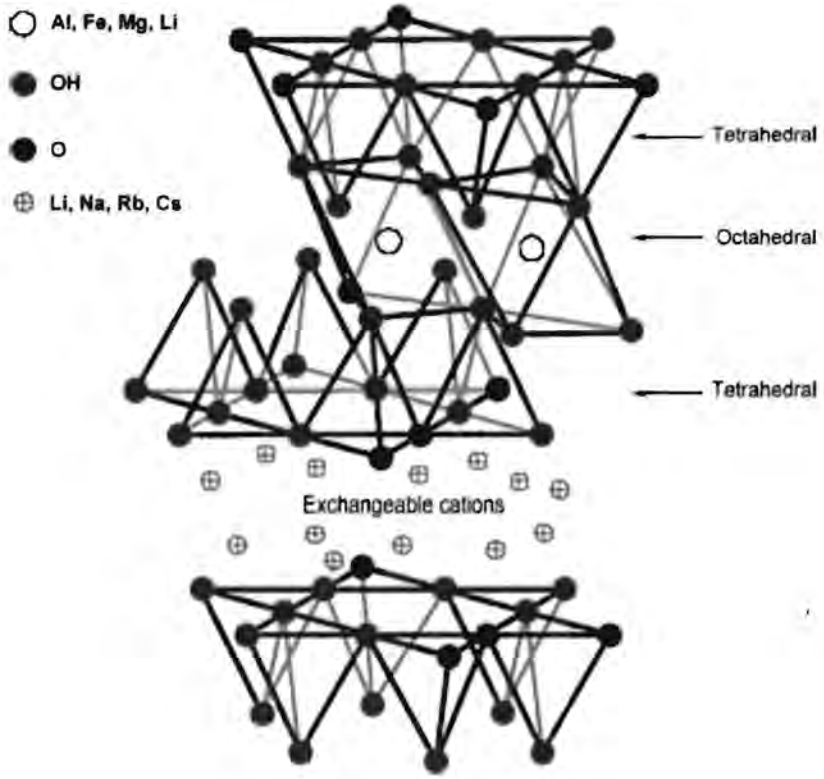

Figure 2.8 Structure of 2:1 layer silicate (Pavlidou, 2008).

2.6 Porous Clay Heterostructure (PCH)

Porous clay heterostructure (PCH) is a porous material that has been developed due to the special properties i.e. improves the ability of adsorption by high surface area. PCH can be prepared by using surfactant incorporated within the galleries of clay. Cationic surfactants will intercalate between the sheets of clay. Then PCH is synthesized by polymerization of the silica source such as

tetraethoxysilane (TEOS) in the presence of surfactant micelles. However, in the preparation of PCH, calcination at high temperature (600-650°C) or solvent extraction method are necessary to remove the surfactant in order to obtain complete silica structure.

Mattayan *et al.* (2009) prepared porous clay heterostructure (PCH) at various ratios of dodecylamine and TEOS and modified the PCH surface by Fe ions (Fe^{2+} and Fe^{3+}). Subsequently, PCH was blended with polylactide to obtain polylactide-clay nanocomposites for food packaging application. The results showed that PCH had surface area of 418-688 m^2/g depending on the various molar ratios of dodecylamine and TEOS. Moreover, magnetic PCH exhibited the bacteriostatic effect against Escherichia coli and Staphylococcus aureus.

To produce porous clay heterostructure with organic-inorganic hybrid structure, the structure of inorganic frame works is combined with organic group in PCH in order to provide the high adsorption property for gas molecules and high selectivity for organic compound.

Srithammaraj *et al.* (2011) prepared porous clay heterostructure (PCH) by the surfactant directed assembly of mesostructured silica within the two-dimensional galleries of clays. PCH was synthesized by the polymerization of tetraethoxysilane (TEOS) in the presence of surfactant micelles within the galleries of bentonite. Moreover, porous clay was modified with organic group (methyltriethoxysilane and 3-mercaptopropyl triethoxysilane) by co-condensation method with TEOS to produce organic-inorganic hybrid material, HPCH and MPPCH respectively. Then, the synthesized PCH, HPCH and MPPCH were blended with polypropylene (PP) to produce PCH/PP, HPCH/PP and MPPCH/PP for ethylene scavenging blown films. From the surface characterization, surface area of PCH, HPCH and MPPCH increased to 507.7, 500.3 and 488.7 m^2/g compared with bentonite which had surface area of 31 m^2/g. In addition, PCH, HPCH and MPPCH showed higher efficiency in adsorbing ethylene gas than bentonite due to the non-polar property of organic group. The amount of ethylene adsorption is in order: HPCH >MPPCH > PCH > BTN. HPCH showed the highest amount of ethylene adsorption because of the similarity of the methyl group in HPCH and ethylene gas.

Recently, aminopropyltriethoxysilane (APTES) are widely used in many applications of surface-modified silica source in order to enhance the properties for the desired application.

Wu *et al.* (2006) modified the surface of submicrometer silica spheres from TEOS with aminopropyl and phenyl groups through one-step process. The particles modified with aminopropyl groups (APTES particles) showed higher organic dye (brilliant blue FCF or BBF) adsorption compared with pure TEOS particle and the particle modified with phenyl group (PhTES particles). The adsorption capacity of the particles increases greatly after acidification because the protonation of silanol groups and amine groups on the particle surface enhanced electrostatic attractions with BBF anions. The APTES particles showed the highest adsorption due to the hydrophobic attractions and the electrostatic attraction from amino group as shown in Figure 2.9.

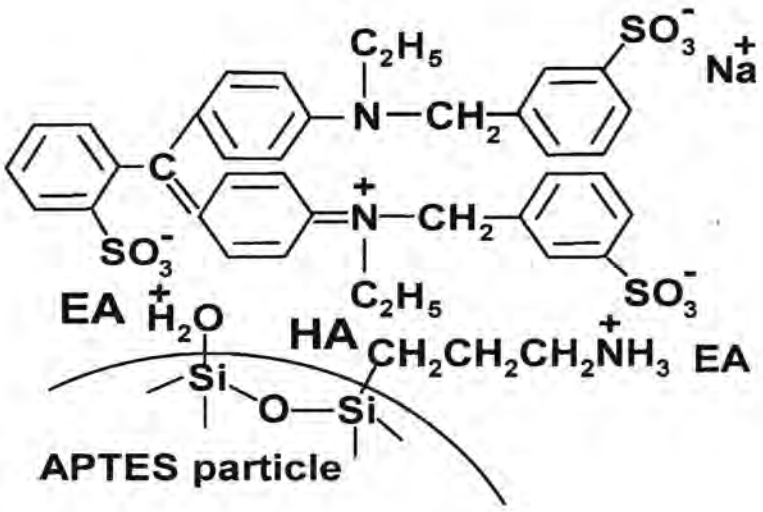

Figure 2.9 Schematic diagrams for the adsorption of BBF by the acidified APTES particles. EA represents electrostatic attraction and HA represents hydrophobic attraction.

Araki *et al.* (2009) synthesized aminopropyl-functionalized mesoporous silica microspheres (AF-MSM) by one-step modified Stober method. The mesoporous silica surface were modified to aminopropyl groups by co-condensation of tetraethoxysilane (TEOS) with 3-aminopropyltriethoxysilane (APTES) at various

mol% of APTES (APTES = 0, 3, 5, 10, 15 and 20 mol %) and dodecylamine (DDA) was used as the catalyst. FT-IR spectra confirmed the presence of aminopropyl groups in AF-MSM by broad band extending from 2800 to 3400 cm^{-1} corresponding to the stretching vibration of NH_3^+ and also by a peak at 1510 cm^{-1} due to the symmetric bending vibration of $-NH_2$. These peaks increased with increasing APTES content. Moreover, AF-MSM was applied to the carbon dioxide adsorbent. Carbon dioxide adsorption capacities increased with increasing with APTES content.

2.7 Clay/Polymer Nanocomposite

Polypropylene (PP) and polyethylene (PE) are the examples of the widely used plastics in large volume because of the advantage such as low cost and wide range of application. To overcome the disadvantage of PP and PE such as low service temperature and to enhance the thermal stability, trying to improve their properties with nanotechnologies was necessary.

Moreover, due to the advantages over other traditional materials such as barrier properties, the use of clay filler in polymer nanocomposite as food packaging materials has increased. In order to improve the barrier properties, clay-polymer nanocomposites are based on a tortuous path around the clay plates, forcing the gas permeation to travel a longer path to diffuse through the film. The increase in path length is a function of the high aspect ratio of the clay filler. Moreover, the resulting from using clay nanoparticles including increased the mechanical properties and thermal properties in polymer.

Clay/polymer nanocomposites are the mixtures of clay in organic polymer. But the homogeneous dispersion of clay in organic polymers is not easy due to the hydrophilicity of clay surface and hydrophobicity of polymer such as polypropylene and polyethylene. Therefore, compatibilizer is important factor to improve the compatibility between polymer and clay.

Surlyn® is one of the compatibilizer which helps to improve the compatibility between polymer and clay by hydrophobic and hydrophilic part respectively. Surlyn® is produced through the copolymerization of ethylene and methacrylic acid.

Methacrylic acid units can be neutralized with a suitable cation commonly Na^{+} or Zn^{+2} as shown in Figure 2.10.

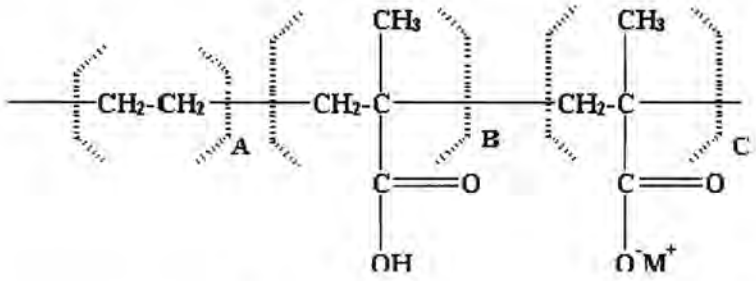

Figure 2.10 Structure of surlyn®.

Tassanawat *et al.* (2007) prepared pH sensitive material used for milk packaging based on polypropylene/organoclay nanocomposites incorporated with indicator dyes using surlyn® as a compatibilizer. The nanoclay composites were fabricated into the sample sheet for color testing and characterizations of thermal and mechanical properties. The results showed that the color of bromothymol blue (BTB) type-film turned from green to yellow whereas bromocresol purple (BP) type-film turn from violet to green correlated with total color difference (TCD) values and titratable acidity (TA) values of fresh milk during storage at ambient temperature. In addition, the clay content had the direct effect on the thermal and mechanical properties of the nanocomposite. The samples with 1 and 3 %wt of organoclay showed the highest Young's modulus, strain at break and toughness but PP/organoclay nanocomposites started to drop in all mechanical properties, except the tensile strength, when the organoclay is incorporated more than 3%wt (5 and 7%wt).

Seephueng *et al.* (2008) prepared colored pH sensor for fish freshenss packaging in order to evaluate the freshness of fresh fish spoilage. The processing of pH-sensitive film based on PP/organomodified clay nanocomposites, using surlyn® as a compatibilizer, laminated with the layer of pH dye. Subsequently, the pH fabricated by using spin-coater and was attached to PP/clay nanocomposite films using a laminating machine (at 160°C). The result showed that the total color difference (TCD) values of bromocresol green (BCG) type indicator correlated with

aerobic plate count (APC) and total volatile basic nitrogen (TVB-N) of fresh fish during spoilage and the color of pH sensor change from yellow to green. Moreover, it was found that incorporation of clay (1, 3 and 5 wt %) increased the thermal stability and gas barrier properties of PP. The clay content had the direct effect on the mechanical properties. Young's modulus, stress at break and % elongation at break is highest at the improvement for sample at 1%wt of organoclay. Conversely, all mechanical properties of PP/clay nanocomposite started to drop when the organoclay is incorporated more than 1%wt resulting from agglomeration and impurity of the organoclay.

Shah *et al.* (2006) prepared blown films of nanocomposites prepared from low density polyethylene and a sodium ionomer of poly(ethylene-co-methacrylic acid). The organoclay content and film blowing conditions were varied to determine the effect of platelet concentration, exfoliation and orientation on film properties. Mechanical properties including stiffness, puncture resistance and resistance to tear propagation were evaluated and compared to corresponding properties of unfilled polymer films. Permeability of the films to moisture and common atmospheric gases like oxygen, nitrogen, and carbon dioxide was also measured using standard testing methods. Films prepared from nanocomposites based on the ionomer exhibited greater improvements in mechanical and barrier properties over unfilled polymer compared to similar films prepared from nanocomposites based on LDPE. This is due to the greater degree of organoclay exfoliation achieved in the ionomer compared to LDPE. The addition of 3 wt% MMT to the ionomer increased the tensile modulus of blown films by an average of 50% without sacrificing much tear strength, puncture resistance or film extensibility. Gas permeability in these films was lowered by 40% and moisture transmission rate was reduced by 60%.

Santamaria *et al.* (2012) studied the structure and mechanical properties of blown films of ionomer compatibilized LDPE nanocomposites. Blown films based on low density polyethylene (LDPE) organoclay nanocomposites (NCs) were obtained by melt extrusion followed by film blowing, using a zinc ionomer of poly(ethylene-co-methacrylic acid) (Pema-Zn) as a compatibilizer. The parameters studied were the compatibilizer and the montmorillonite (MMT) contents that ranged from 0 to 20% and from 0 to 5%, respectively. The presence of clay hindered Pema-

Zn crystallization indicating the existence of interaction between the Pema-Zn and the clay. Analysis of the nanostructure showed that the MMT was found inside microscopic domains of Pema-Zn distributed throughout the LDPE matrix. The addition of Pema-Zn improved the dispersion of the clay in LDPE films resulting in synergistic improvements in the mechanical properties. These improvements occur both in the machine and transverse directions. Thus, the presence of Pema-Zn is a determining factor in biaxiality and can clearly be attributed to the bidimensional laminar structure of clays such as MMT.

3. PROCEDURE

3.1 Materials

3.1.1 Clay Mineral

Commercial sodium activated bentonite Mac-Gel® (GRADE SAC), Na-BTN, with cationic exchange capacity (CEC) of 44.5 meq/100 g clay, was supplied by Thai Nippon Co., Ltd. Thailand.

3.1.2 Surfactant

Cetyl trimethyl ammonium bromide (CTAB) was purchased from Italmar Co., Ltd.

Dodecylamine (DDA) was purchased from Aldrich.

3.1.3 Chemical Substances

Tetraethoxysilane (TEOS) was purchased from Aldrich.

3.1.4 Polymer

Low density polyethylene under trade name (PETLIN LD C150Y) (MFI 5 dg/10min) was purchased from PETLIN (MALAYSIA) Sdn Bhd.

3.1.5 Compatibilizer

Sodium-neutralized ethylene-co-methacrylic acid (MFI = 4 dg/10min) under trade name Surlyn® PC350 was purchased from DuPont Co., Ltd.

3.1.6 Indicator

Bromothymol Blue ($C_{27}H_{28}Br_2O_5S$, MW 624.4 g/mol) was purchased from Ajax Finechem, Australia.

3.1.7 Reagent

Hydrochloric acid 37% was purchased from Calro Erba.

Boric acid was purchased from (H_3BO_3) was purchased from Calro Erba.

Potassium carbonate (K_2CO_3) was purchased from Calro Erba.

Trichloroacetic acid (TCA) was purchased from Calro Erba.

3.1.8 Solvent

Methanol was purchased from RCI Labscan Limited.

3.2 Equipment

3.2.1 X-ray Diffractometer (XRD)

The X-ray diffractometer using Bruker AXS model Diffractrometer D8 was used to identify the interlayer spacing of Na-bentonite and modified clay. The experiment was performed in the 2θ range of 2-10 degrees with scan speed 2 degree/min and scan step 0.01 degree.

3.2.2 Fourier Transform Infrared Spectrometer (FT-IR)

The functional group of Na-bentonite and modified clay were identified by Nicolet Nexus 670 FTIR spectrometer. FTIR was carried out in the transmission mode with 64 scans between 4000-400 cm^{-1} at a solution of 4 cm^{-1}.

3.2.3 Scanning Electron Microscope (SEM)

The surface morphology of Na-bentonite and modified clay were observed by using S-4800 field emission scanning electron microscope. Then, the dispersion of the PCH in polymer matrix was determined. The specimens were coated with platinum before observation.

3.2.4 Surface Area Analyser (SAA)

The pore size, surface area and pore volume of porous samples were measured by nitrogen adsorption-desorption isotherms on surface area analyzer using Quantachrome Autosorb-1. The samples were degassed at 250°C for 17 h in a vacuum furnace before analysis.

3.2.5 UV-Vis Spectrometer

The indicator dye (bromothymol blue) was dissolved in water to prepare standard solution. Optical absorption spectrum of standard solution and the solution of leaching of dye from nanocomposite film was observed by UV-Vis using Shimadzu Model UV-1800.

3.2.6 Twin Screw Extruder

The nanocomposites were prepared by using co-rotating twin-screw extruder (Labtech) with L = 80 and D = 20 mm. The operation temperature was performed at 170, 175, 180, 185, 190, 195, 200, 205, 210 and 215°C from hopper to die respectively and the screw speed was 25 rpm for prepared LDPE/Clay nanocomposites.

3.2.7 Compression Molding Machine

The nanocomposite films were prepared by compression molding machine using Wabash V50H. The mold containing the pellet was preheated at 130°C for 5 minutes and then compression at 5 tons of force for 5 minutes for prepared LDPE/Clay nanocomposite films. Then, the molds were cooled to 50°C.

3.2.8 Gas Permeability Testing

Oxygen Permeation Tester, Illinois model 8000, was used to determine the oxygen gas transmission rate through LDPE films and LDPE/clay nanocomposite films. Gas permeation experiment was investigated following the procedure described in ASTM D 3985-05 at 23°C. The films were prepared by compression molding and were cut into circular shape with 15 cm in diameter.

3.2.9 Calorimetric Spectrophotometer

The nanocomposite films were measured the color change by the HunterLab Model Colorflex with 45°/0° optical geometry and EasyMatch® QC software. The result was expressed as Hunter color system (L, a, b) values and total color difference (TCD) or ΔE. The nanocomposite films were cut into the circular shape with diameter of 4 cm. The TCD value was calculated by following equation:

$$\Delta E = [(\Delta L)^2 + (\Delta a)^2 + (\Delta b)^2]^{1/2}$$

Where, ΔL = The brightness difference between sample and target

Δa = The redness difference between sample and target

Δb = The yellowness difference between sample and target

The target color is (93.13, -0.96, 1.69) corresponding to (L, a, b) for white standard color in Hunter system.

3.2.10 Thermogravimetric Analyzer (TGA)

Thermogravimetric analysis (TGA) was used to study the thermal stability of LDPE/clay nanocomposite films compared to LDPE films. The degradation temperature of samples was determined by Perkin Elmer Pyris Diamond TG/DTA instrument. The pellets were loaded on platinum pan and heated from 30 to 900°C at heating rate 10°C/min and flow under N_2 200 ml/min.

3.2.11 Differential Scanning Calorimeter (DSC)

The crystallization and melting behavior of LDPE/clay nanocomposite films compared to LDPE films were measured by Differential Scanning Calorimeter (DSC) using Met.ler DSC822 STARe System. First, the pellet samples was heated from 30°C to 200°C at heating rate of 10°C/min in order to eliminate the influence of thermal history and then cooled down from 200°C to 30°C to observe melt crystallization behavior. After that, reheated to 200°C to observe melting behavior.

3.2.12 Lloyd Universal Testing Machine

Tensile test of nanocomposite films was measured under ASTM D 683. The specimen was cut into rectangular shape with 10x100 mm and cross head speed of 50 mm/min.

3.3 Methodology

3.3.1 Preparation of Climacteric Fruit Freshness Indicator

3.3.1.1 Preparation of Porous Clay Heterostructure (PCH)

The obtained organoclay prepared with the surfactant (Cetyl trimethyl ammonium chloride, CTAC) was added to a neutral amine such as dodecylamine and tetraethoxysilane (TEOS) in the follow molar ratio: organoclay/dodecylamine/TEOS = 1/20/150. In first step, organoclay was mixed with dodecylamine and stirred at 50°C for 30 min. After that tetraethoxysilane (TEOS) was added to the mixture allowed reacting for 4 h at room temperature under continuous stirring. After reaction, the modified clay was filtrated from the solution and washed with methanol. The modified clay was dried at room temperature for 24 h. For extraction process, 1 g of as-synthesized PCH was added to 45 ml of methanol and 5 ml of concentrated HCl and refluxed for 2 h. Then, the modified clay was filtered off and washed with methanol and water. After that, it was air-dried at room temperature overnight before screened through a mesh #325.

The interlayer spacing of modified clay was studied by small angle X-ray diffractometer. The intercalation of cationic surfactant between the layers of bentonite was studied using FTIR spectra.

The surface morphology of porous clay compared to the pristine clay was observed by SEM images. The pore diameter, pore volume and surface area of porous clay compared to the pristine clay were characterized by surface area analyzer.

3.3.1.2 Preparation of Chromophores Modified PCH

The PCH was modified with pH dye (bromothymol blue) at weight ratio of PCH: dye of 10:1, 20:1 and 30:1. First, bromothymol blue was dissolved in solution of 0.05 M NaOH. Then, bromothymol blue solution was added into the PCH under continuous stirring to obtain chromophores modified PCH. After that the modified clay was filtered off and dried in vacuum oven before screened through a mesh #325. The bromothymol blue modified PCH was named PCH-BTB.

The morphology of PCH-BTB was observed by SEM images. The results of pore diameter, pore volume and surface area after incorporated bromothymol blue onto PCH were measured by surface area analyzer.

3.3.1.3 Preparation of Nanocomposite Film

The nanocomposite was prepared by using twin-screw extruder (Labtech) with L = 80 and D = 20 mm. The operation temperature was performed at 130°C from hopper to die respectively and the screw speed was 25 rpm.

First, low density polyethylene (LDPE) was blended with 6%wt surlyn® in order to obtain LDPE/surlyn® pellet. Then, LDPE/surlyn® pellet was mixed with 2 %wt of chromophores modified PCH to obtain the nanocomposite. Each composition was dried in vacuum oven for moisture removal and premixed in tumble mixer before extruded through the twin screw extruder. Then, the extruded nanocomposite was quenched immediately in water and pelletized. The obtained pellet was dried in vacuum oven.

Nanocomposite films of LDPE/chromophores modified PCH was prepared by compression molding machine at 5 tons of force for 5 minutes. The processing temperature was 130°C.

3.3.1.4 Indicator Films Response to Standard Carbon dioxide

The main products from respiration of climacteric fruits such as carbon dioxide and water were used to test the sensitivity of color response of indicator films. The indicator film was placed in glass chamber with contained

standard carbon dioxide and water. Standard carbon dioxide in various concentrations (0, 30, 60, 90, 120 and 150 ppm) and the excess water was prepared into 600 ml glass chamber. Then, the glass chamber was closed by the rubber stopper with the rubber septum in the middle of the stopper. Color changes of indicator film at weight ratio of PCH: dye of 10:1, 20:1 and 30:1 after reacted with carbon dioxide and water was measured by the calorimetric spectrophotometer. The result was expressed as Hunter color system (L, a, b) values and total color difference (TCD) or ΔE.

3.3.1.5 Leaching Studies

Indicator dye (bromothymol blue) was dissolved in water to prepare standard solutions of 1, 2, 5 and 10 ppm. Then the absorbance of standard solution was investigated by UV-Vis Spectroscopy (Shimadzu Model UV-1800). The indicator nanocomposite films were cut into the rectangular shape with 4x4 cm and soaked with 10 ml of water in a small container for approximately 48 h. Then, the wavelength spectrum in range of 400 to 700 nm was carried out to detect the presence of bromothymol blue.

4. RESULTS AND DISCUSSION

4.1 Charactrization of the organomodified bentonite (OBTN), Porous Clay Heterostructure (PCH) and Functionalized Porous Clay Heterostructure (APPCH)

The sodium bentonite clay (Na-BTN) and the obtained modified clay (OBTN, PCH and APPCH) were shown in Figure 4.1.

(a) (b) (c) (d)

Figure 4.1 (a) Na-BTN, (b) OBTN, (c) PCH and (d) APPCH.

The organomodified bentonite (OBTN) was confirmed the expansion of sodium bentonite (Na-BTN) layers by incorporating of cationic surfactant and studied the effect of using different surfactant by XRD. Figure 4.2 showed XRD results of Na-BTN and OBTN. The XRD pattern showed the presence of the (001) reflection peak. The d_{001} peak of Na-BTN at $2\theta = 7.10°$ which corresponded to the basal spacing of 1.24 nm (Figure 4.2 a). After modified Na-BTN with cationic surfactant, cetyl trimethyl ammonium bromide (CTAB), OBTN showed the d_{001} peak at lower angle of 2.25° which corresponded to the basal spacing of 3.93 nm (Figure 4.2 b) indicating the increasing the basal spacing of clay layers due to ammonium ions from cationic surfactant intercalated into the silicate layers. In addition, the XRD result showed that the obtained OBTN synthesized from the surfactant, cetyl

trimethyl ammonium chloride (CTAC) as shown in Figure 4.2 c showed the increasing the basal spacing of clay layers but the d-spacing less than the OBTN synthesized from CTAB [1].

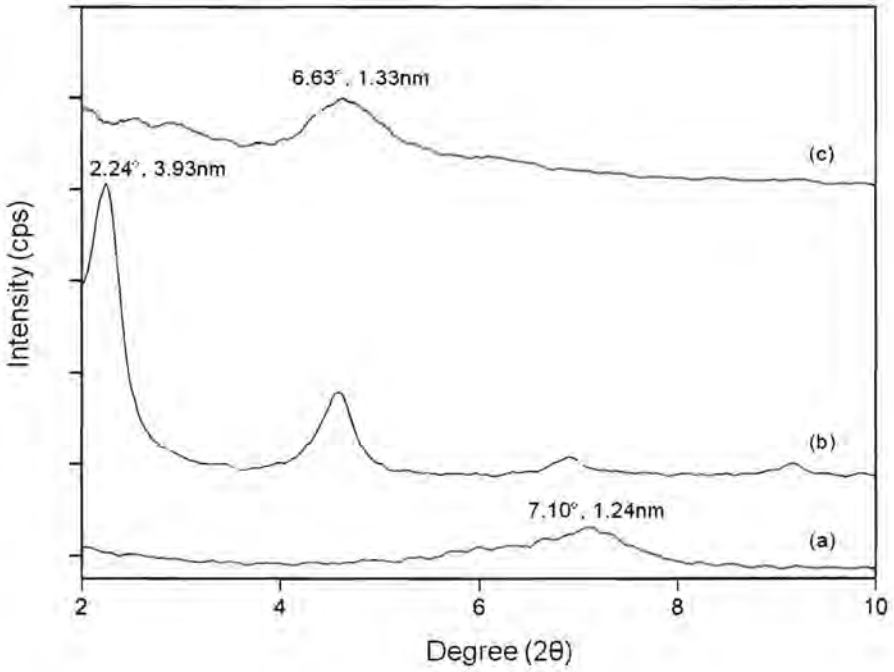

Figure 4.2 The XRD patterns of (a) Na-BTN, (b) OBTN (CTAB) and (c) OBTN (CTAC).

From the FTIR results (Figure 4.3), the FTIR spectrum of Na-BTN (Figure 4.3 a) showed the peak at around 3500 cm^{-1} assigned to the stretching vibration of the silanol associated with the silica structure and the peak at around 1000 cm^{-1} assigned to the stretching vibration of the SiO_4 units. The peaks at around 1100 and 800 cm^{-1} were assigned to the asymmetric and symmetric stretching vibrations of the Si-O-Si linkage. The presence of surfactant in the layer of BTN was indicated by FTIR spectra of OBTN (Figure 4.3 b). The peaks at 2919 and 2850 cm^{-1} were assigned to asymmetric and symmetric stretching vibrations of methyl and methylene groups of hexadecyltrimethylammonium ion respectively. The FTIR spectra of PCH (Figure 4.3 c) and APPCH (Figure 4.3 d) were different from Na-BTN at the absence of the peak at 1000 cm^{-1} because of the changing of clay structure after modification.

In addition, the peak at around 1510 cm^{-1} were confirmed the organic group ($-NH_2$) from APTES molecule in the structure of APPCH [2].

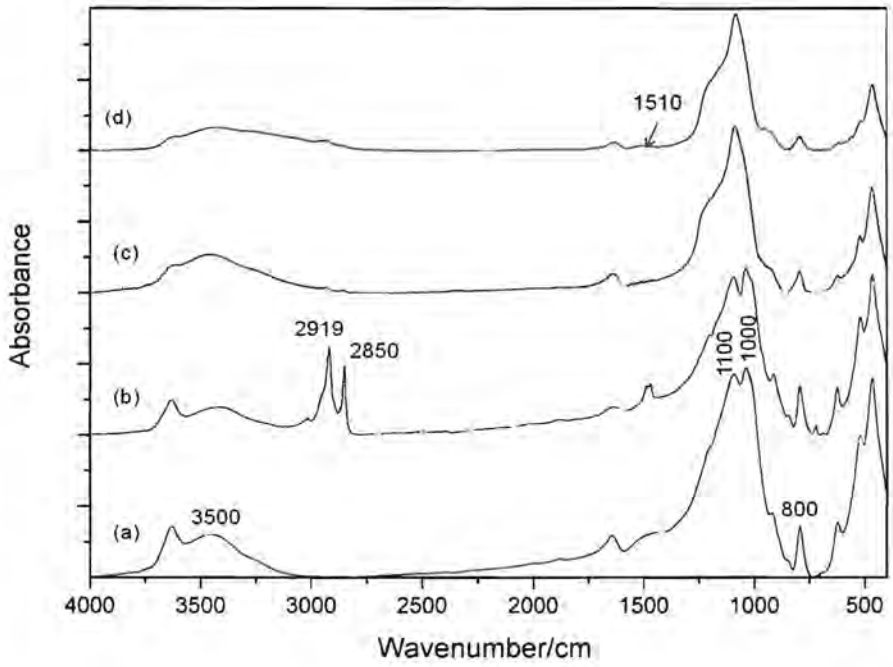

Figure 4.3 Fourier transform infrared spectroscopy spectra of (a) Na-BTN, (b) OBTN, (c) PCH and (d) APPCH.

The morphology of Na-BTN and modified clay were characterized by SEM image. The flat plate structure of Na-BTN was observed (Figure 4.4 a). After porous samples were synthesized within the galleries of bentonite by the polymerization of tetraethoxysilane (TEOS) in the presence of surfactant micelles, the rugged surface of PCH (Figure 4.4 b) and APPCH (Figure 4.4 c) were presented because of the formation of pore structure in the galleries of clay [3].

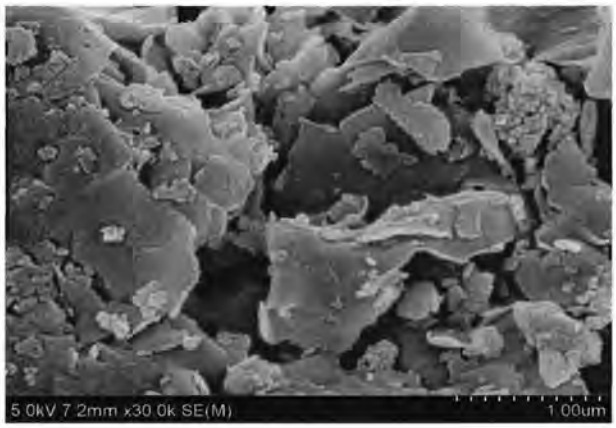

(a)

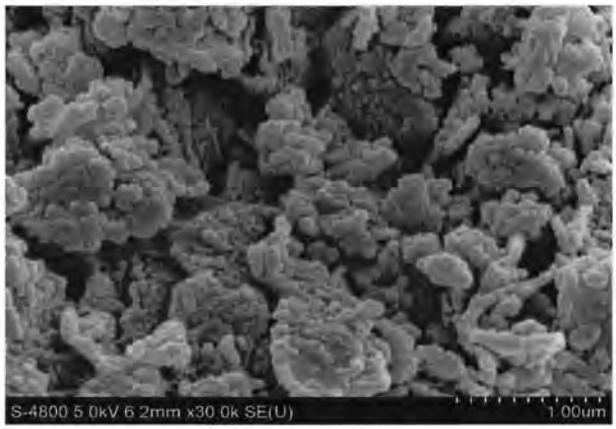

(b)

Figure 4.4 Scanning electron microscope images of (a) Na-BTN, (b) PCH.

The results from nitrogen adsorption-desorption (Table 4.1) showed the increasing of specific surface area of porous material (PCH and APPCH) compared with Na-BTN. The results revealed that PCH had the high surface areas of 524.1 m^2/g, average pore diameter of 4.85 nm and pore volume of 0.64 cc/g. While the functionalized PCH (APPCH) with amino group ($-NH_2$) had the decrease of surface area and pore volume compared to PCH and the increasing of APTES content reduced surface area and pore volume. The values of surface area and pore volume were in the range of 119.8-320.5 m^2/g and 0.33-0.42 cc/g, respectively. The results indicated that the incorporation of amino group ($-NH_2$) in porous structure was successful [3, 4, 5].

Table 4.1 Surface area, pore diameters and pore volume from nitrogen adsorption-desorption

Sample	Multipoint BET surface area (m^2/g)	Average pore diameter (nm)	Pore volume (cc/g)
Na-BTN	31.0	-	-
PCH	524.1	4.85	0.64

4.2 Characterization of Chromophores Modified PCH

The morphology of the chromophores (bromothymol blue) modified PCH, was determined by nitrogen adsorption-desorption and the results were reported in Table 4.4. The results showed that the surface area and pore volume of PCH decreased while the average pore diameter increased after modification the porous sample with pH dye. The chromophores modified PCH (PCH-BTB) had the surface area of 32-57 m^2/g, average pore diameter in range of 20.12-25.77 nm and pore volume of 0.21-0.29 cc/g. The large decrease of surface area and increase of average pore diameter of PCH after modification with pH dye indicated that the large molecule of bromothymol blue incorporated into the structure of PCH and the amount of dye content not have the influence to decrease the surface area.

The chromophores (bromothymol blue) modified PCH were prepared as shown in Figure 4.5.

Table 4.2 Surface area, pore diameters and pore volume from nitrogen adsorption-desorption

Sample	Multipoint BET surface area (m^2/g)	Average pore diameter (nm)	Pore volume (cc/g)
PCH	524.1	4.85	0.64
PCH-BTB (10:1)	37.73	23.65	0.22
PCH-BTB (20:1)	57.21	20.12	0.29
PCH-BTB (30:1)	32.94	25.77	0.21

10:1 20:1 30:1

Figure 4.5 Bromothymol blue modified PCH at various weight ratio of clay and pH dye; 10:1, 20:1 and 30:1.

The XRD patterns of the PCH and chromophores modified PCH (PCH-BTB) was shown in Figure 4.6 (a) – (d). The results showed that there was no obvious peak observed in XRD patterns of PCH. While the XRD patterns of PCH-BTB showed the peaks around 2θ = 6.6 nm which corresponded to the basal spacing about 1.3 nm might be due to the formation of the partial layer structure of PCH after modified with bromothymol blue.

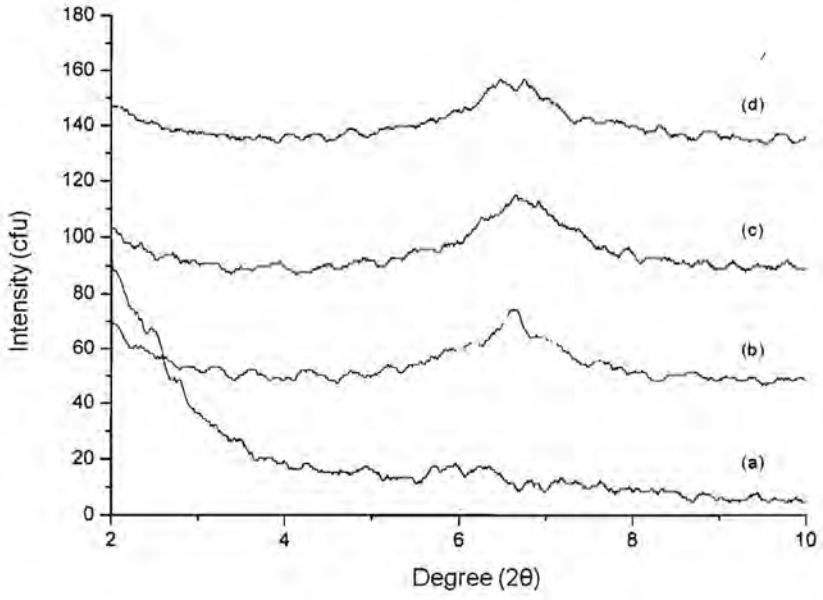

Figure 4.6 The XRD patterns of (a) PCH, (b) PCH-BTB 10:1, (c) PCH-BTB 20:1 and (d) PCH-BTB 30:1

The results of SEM image as shown in Figure 4.7 indicated that the rugged surface of PCH after modified with chromophore (bromothymol blue) still remained.

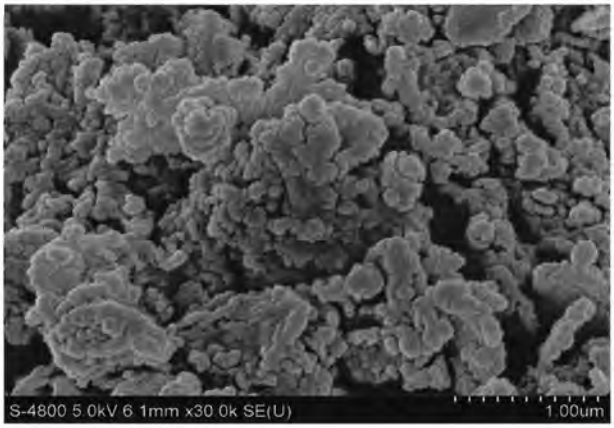

(a)

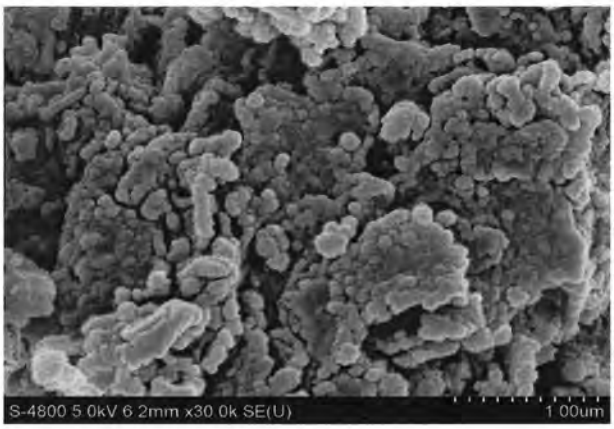

(b)

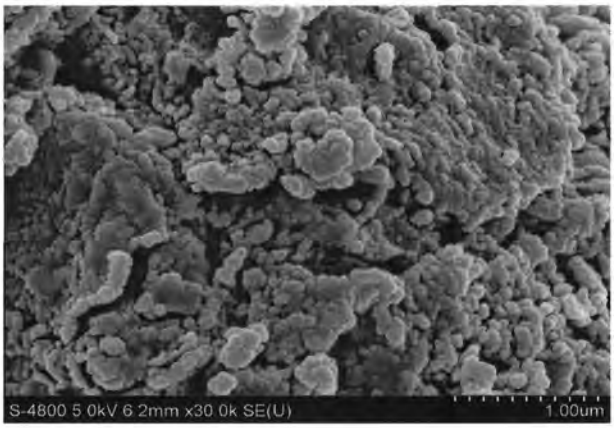

(c)

Figure 4.7 SEM images of (a) PCH-BTB 10:1, (b) PCH-BTB 20:1 and (c) PCH-BTB 30:1.

4.3 pH Indicator Film Response to Standard CO_2 and H_2O

Because the ripening of climacteric fruit associates with increasing in respiration and the main products from respiration of climacteric fruits such as carbon dioxide and water are generally to measure. Thus, carbon dioxide and water releasing before climacteric peak at the time that the fruit starts to ripen is the most important parameter to evaluate the freshness of the climacteric fruit by the color change of pH indicator films [3].

The color change of indicator films (LDPE/PCH-BTB nanocomposite films) after test with excess water and standard carbon dioxide (CO_2) at concentration from 0 to 150 ppm which can be compared with the production of CO_2 in the preclimacteric to climacteric phase during fruit ripening was shown in Table 4.3, Table 4.4, Table 4.5 and Figure 4.8. The result showed that the color of indicator film changed the color from green to yellow correlated with increasing in standard CO_2 levels as shown in Figure 4.9. The total color difference (ΔE) and hunter b values continuously increases at low concentration of standard CO_2 and remaining constant at high concentrations due to the saturation of color change. Moreover, the pH indicator film PCH-BTB 10:1 showed the highest sensitivity of color change compared to PCH-BTB 20:1 and PCH-BTB 30:1 at low concentrations of standard CO_2. The reaction of color change was described. Carbon dioxide combined with water and producing carbonic acid. Carbonic acid dissociated from parent molecule forming hydrogen ions (H^+) and bicarbonate ion (HCO^{3-}). Then, as a proton, a hydrogen ion combined with water molecule to form a hydronium ion (H_3O^+). Hydronium ions reacted with the bromothymol blue in basic form resulting in an acid form. The color change of indicator film was presented. The mechanism of color change was shown in Figure 2.7. Therefore, this pH indicator film can be applied for detecting the quality of climacteric fruit by color change.

Table 4.3 Change in hunter color (L, a, b) and total color difference (TCD) values of LDPE/PCH-BTB (10:1) nanocomposite films after indirect contact with standard carbon dioxide and excess water

Concentration (ppm)	L	a	b	ΔL	Δa	Δb	ΔE
30	29.83	-5.45	3.03	-1.06	0.27	0.65	1.19
60	29.28	-6.61	3.75	0.52	0.5	1.53	1.69
90	28.42	-5.83	2.92	0.35	0.36	2.25	2.31
120	28.56	-5.48	2.86	0.79	0.47	2.00	2.20
150	29.05	-5.28	2.40	0.03	0.63	2.08	2.17

Table 4.4 Change in hunter color (L, a, b) and total color difference (TCD) values of LDPE/PCH-BTB (20:1) nanocomposite films after indirect contact with standard carbon dioxide and excess water

Concentration (ppm)	L	a	b	ΔL	Δa	Δb	ΔE
30	32.75	-6.73	1.42	0.55	0.32	0.30	0.70
60	32.28	-5.65	1.06	0.15	0.33	1.18	1.23
90	32.41	-5.78	1.08	-0.21	0.16	1.54	1.56
120	31.69	-6.08	0.62	0.36	0.56	2.01	2.12
150	32.23	-5.62	0.70	-0.12	0.32	2.15	2.18

Table 4.5 Change in hunter color (L, a, b) and total color difference (TCD) values of LDPE/PCH-BTB (30:1) nanocomposite films after indirect contact with standard carbon dioxide and excess water

Concentration (ppm)	L	a	b	ΔL	Δa	Δb	ΔE
30	32.53	-5.87	1.64	-0.02	0.08	0.33	0.35
60	31.27	-5.39	0.70	-0.04	0.17	1.23	1.24
90	33.37	-5.97	1.18	-1.18	-0.17	2.05	2.37
120	33.15	-5.80	1.10	0.50	0.09	2.24	2.49
150	31.19	-5.70	0.78	0.16	0.16	2.23	2.24

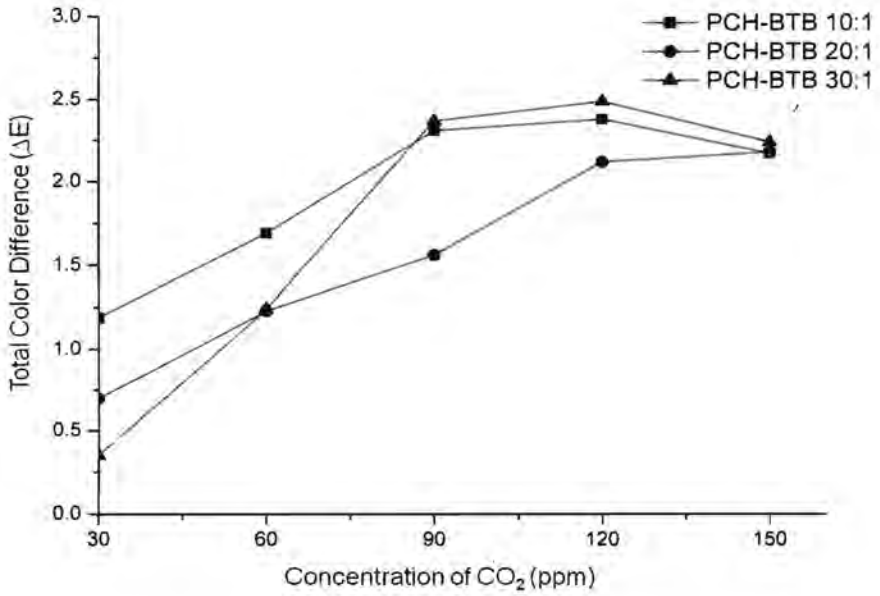

Figure 4.8 Changes in total color difference values (ΔE) of pH indicator film at various weight ratio of PCH: BTB (a) 10:1 (b) 20:1 and (c) 30:1.

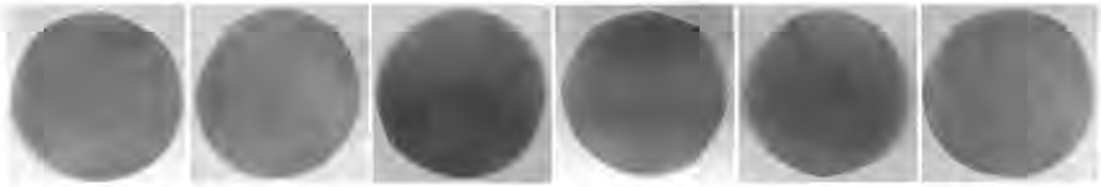

(a) (b) (c) (d) (e) (f)

Figure 4.9 Color changes of LDPE/PCH-BTB (10:1) nanocomposite films after test with standard carbon dioxide at various concentrations (a) 0 ppm (b) 30 ppm (c) 60 ppm (d) 90 ppm (e) 120 ppm and (f) 150 ppm.

4.4 pH Indicator Film Response to Fresh Banana

The result of indicator film response after in direct contact with fresh banana was observed. The pH change during storage was shown in Figure 4.10. The result showed that the color of indicator film changed the color from green to yellow when banana started to ripen and remained constant due to the saturation of color as shown in Figure 4.11 and 4.12.

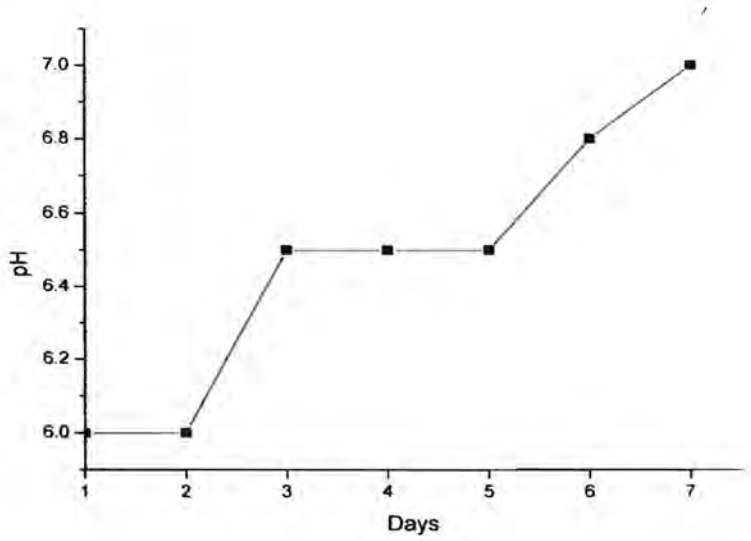

Figure 4.10 Changes in pH of fresh banana during storage at room temperature.

Figure 4.11 Reference bananas ripening at room temperature.

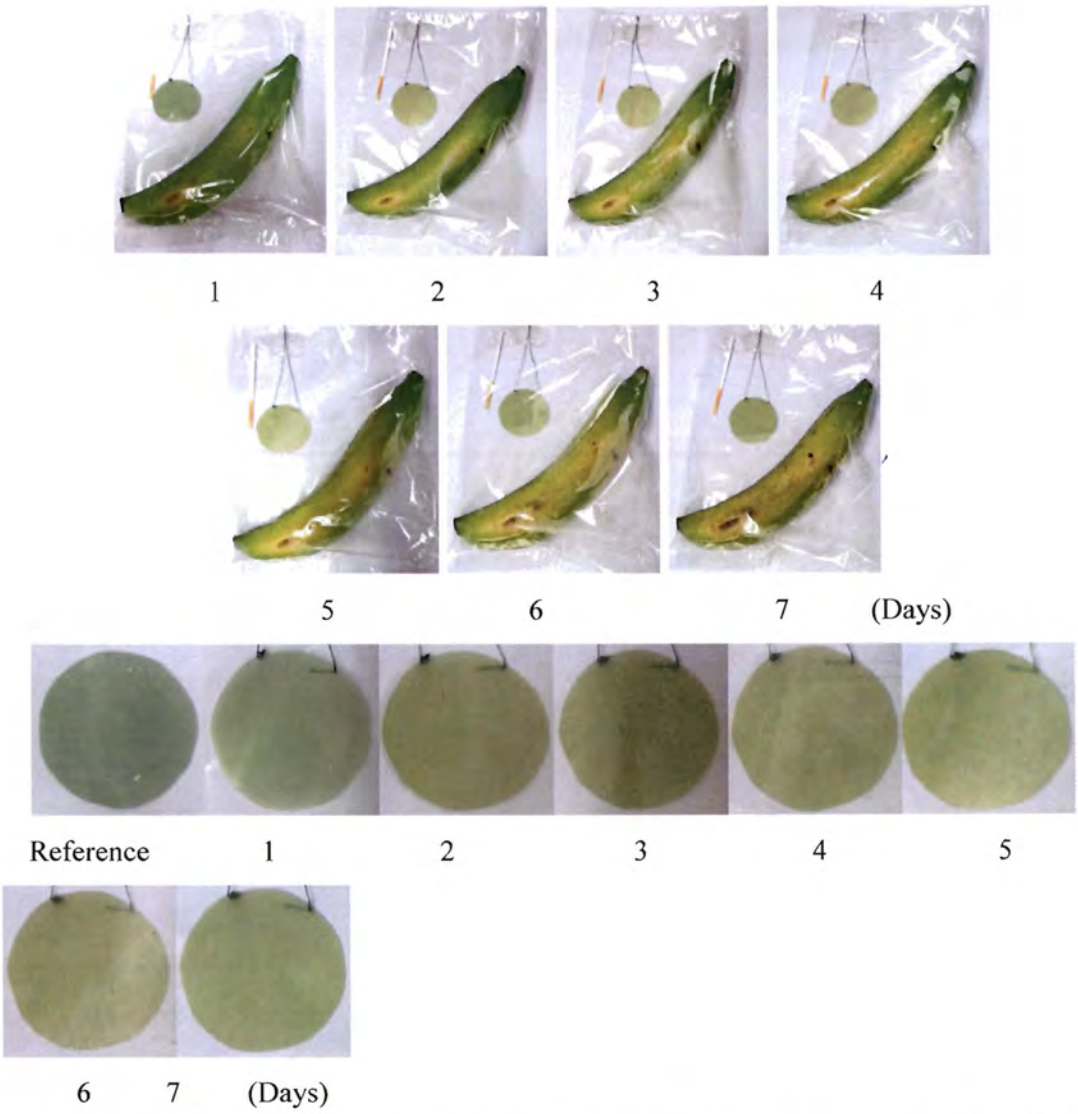

Figure 4.12 Color change of LDPE/PCH-BTB (10:1) nanocomposite film during banana ripening.

4.5 Leaching Studies

The leakage of the indicator dyes from the LDPE/PCH-BTB nanocomposite films with calibration curves was observed by UV-Vis spectrometer as shown in Figure 4.14, respectively. After the both indicator films were soaked in water and carried out to detect the presence of pH dye. The results showed that the absorbance of water was about zero equaled to the absorbance of reference distill water. Thus, the results indicated that no have leakage of bromothymol blue from both pH indicator films.

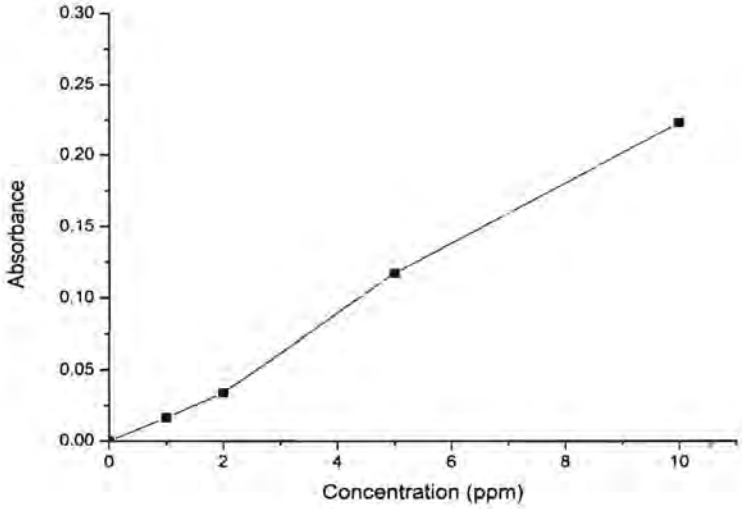

Figure 4.13 The leakage of bromothymol blue from LDPE/PCH-BTB nanocomposite films

4.6 Thermal Behavior of Nanocomposites

The crystallization temperature and melting temperature were measured by DSC. The result showed that the crystallization temperature of LDPE/PCH-BTB nanocomposites remained constant. The melting temperature of LDPE/PCH-BTB nanocomposites closed to neat LDPE. Moreover, the results indicated that the crystalline and melting characteristics of nanocomposites were not dependent on dye content. DSC thermograms of nanocomposites are shown in Figure 4.15.

The thermal degradation temperature was measured by TGA. TG-DTA curves were shown in Figure 4.16. The results showed that the thermal degradation occurred in single stage. The nanocomposites showed the higher thermal stability than neat LDPE. This behavior may be attributed to the formation of a high-performance carbonaceous silicate char build up on the surface [2].

Melting, crystallization and thermal behavior results are shown in Table 4.6 and 4.7.

Table 4.6 Melting and crystallization behavior

Sample	T_C (°C)	T_m (°C)	ΔH_m (J/g)	%Crystallinity
LDPE	95.01	109.10	69.58	33.29
LDPE/6%wtSurlyn	95.22	109.31	76.67	36.68
LDPE/6%wtSurlyn/2%wtPCH-BTB(10:1)	95.78	108.76	70.52	33.74
LDPE/6%wtSurlyn/2%wtPCH-BTB(20:1)	95.28	109.27	71.46	34.19
LDPE/6%wtSurlyn/2%wtPCH-BTB(30:1)	95.57	109.29	71.08	34.01

Table 4.7 Thermal behavior

Sample	Char residue (%wt)	T_d (°C)
LDPE	1.2	449.0
LDPE/6%wtSurlyn	0.2	450.7
LDPE/6%wtSurlyn/2%wtPCH-BTB(10:1)	2.9	451.9
LDPE/6%wtSurlyn/2%wtPCH-BTB(20:1)	5.0	449.0
LDPE/6%wtSurlyn/2%wtPCH-BTB(30:1)	2.6	453.0

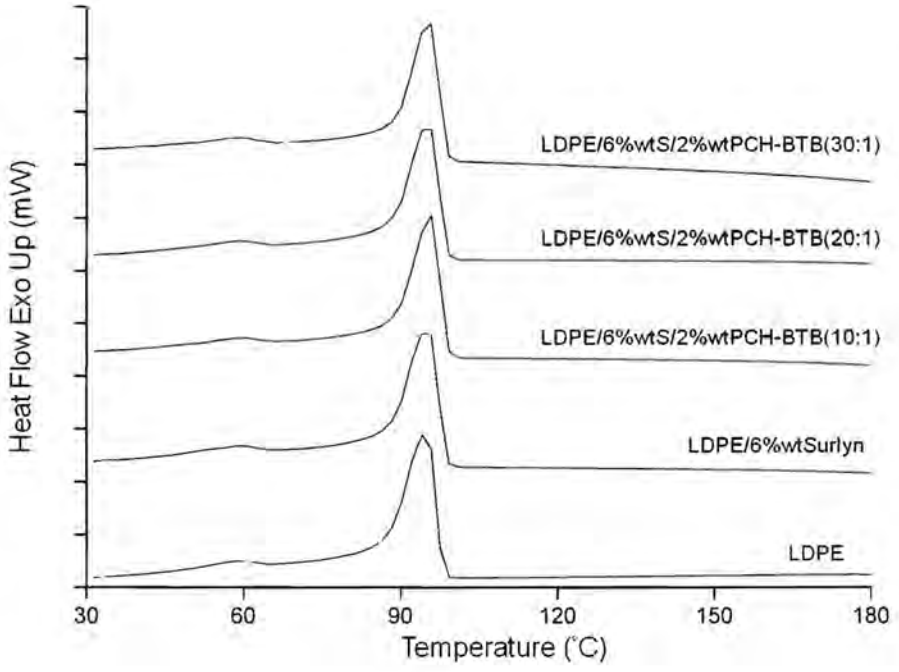

(a)

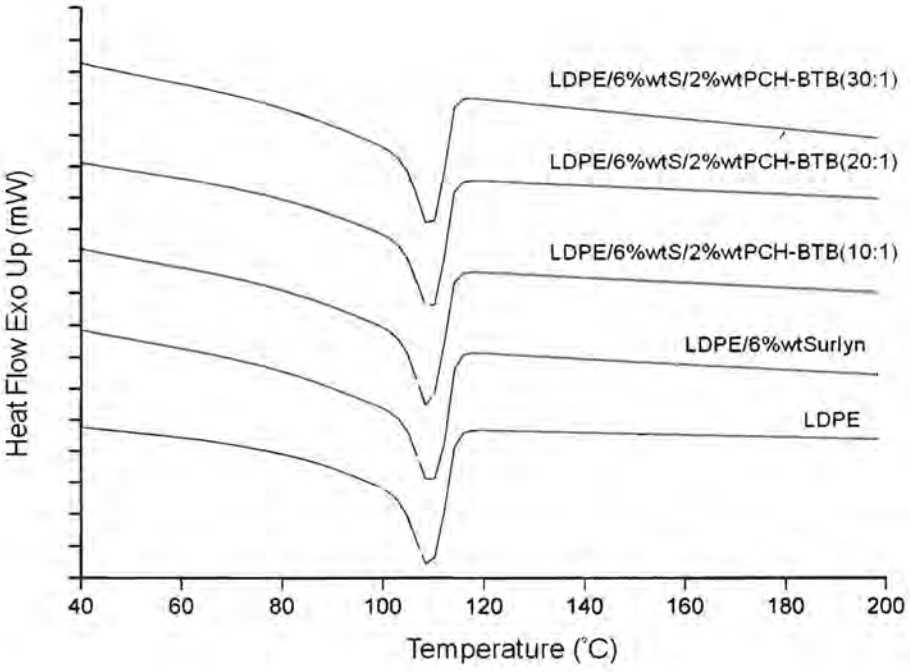

(b)

Figure 4.14 DSC thermograms of LDPE/PCH-BTB nanocomposites (a) crystallization temperature and (b) melting temperature.

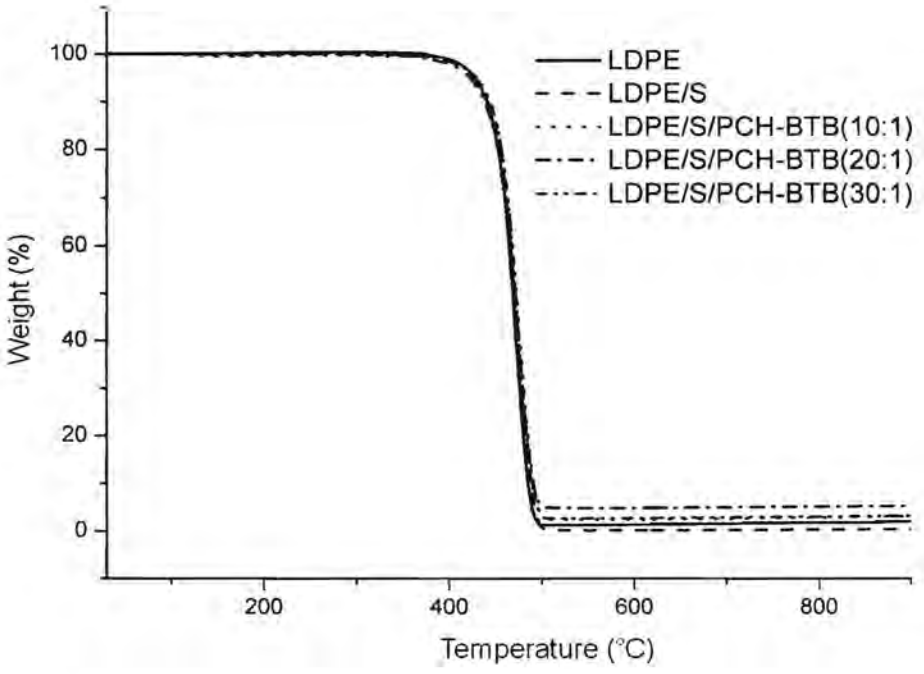

Figure 4.15 TG curves of LDPE/PCH-BTB nanocomposites

4.7 Mechanical Properties of Nanocomposites

The mechanical properties of LDPE/PCH-BTB nanocomposite films compared to neat LDPE were shown in Figure 4.17, 4.18 and 4.19. The result showed that Young's modulus and tensile strength increased in the presence of clay in nanocomposite films due to the porous clay acting as the excellent filler with enable to reinforce the films. While % elongation at yield decreased in the presence of clay in nanocomposite films. The possible reason may be due to the addition of clay was attributed to increase stiffness of polymer [6].

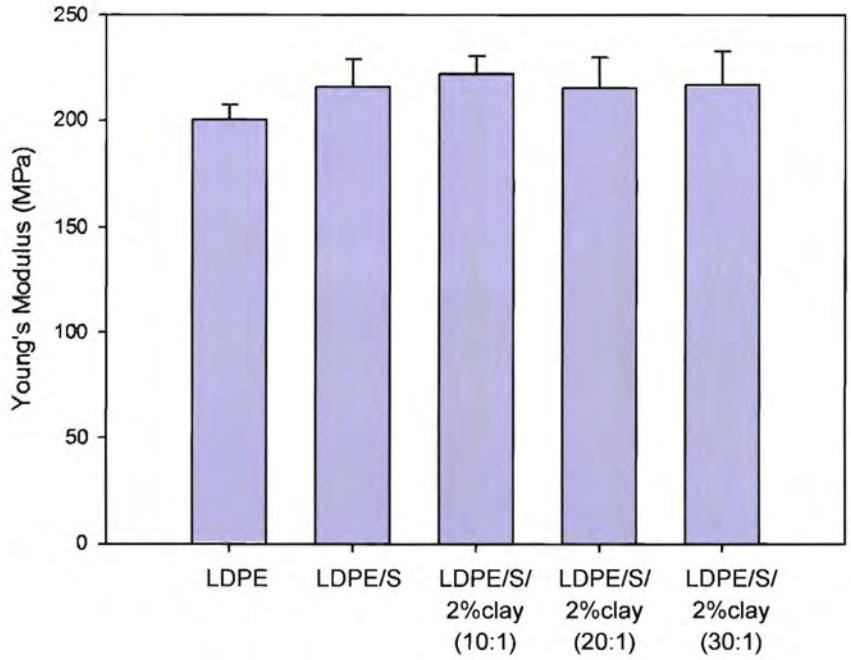

Figure 4.16 Young's modulus of LDPE and LDPE/PCH-BTB nanocomposite films.

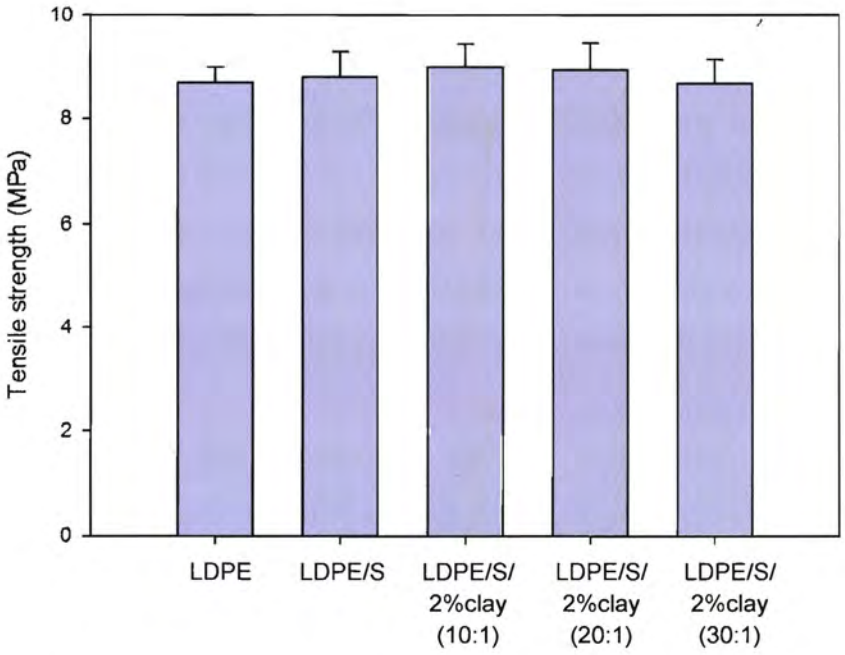

Figure 4.17 Tensile strength of LDPE and LDPE/PCH-BTB nanocomposite films.

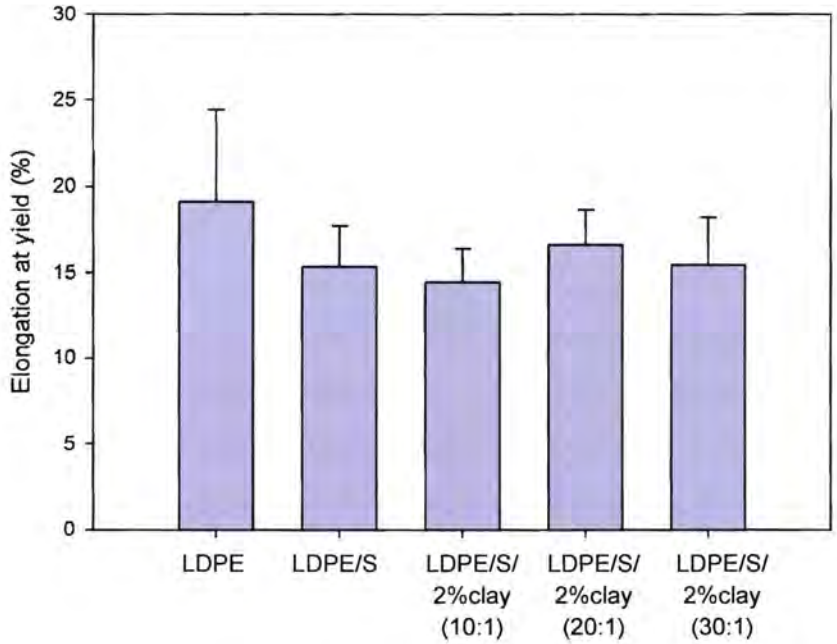

Figure 4.18 % Elongation at yield of LDPE and LDPE/PCH-BTB nanocomposite films.

4.8 Oxygen Gas Permeability of Nanocomposite Films

Oxygen gas transmission rate of nanocomposites was shown in Table 4.8. The results showed the reduction of oxygen transmission rate in nanocomposites compared to neat LDPE. Porous clay improved the barrier properties of nanocomposite indicated by the reduction of oxygen transmission rate in the nanocomposites. The improvement in barrier properties of nanocomposites was due to the presence of porous clay which provided the tortuous path in polymer matrix.

Table 4.8 Oxygen gas transmission rate of LDPE and LDPE/PCH-BTB nanocomposites

Sample	Oxygen gas transmission rate ($cc/m^2.day$)
LDPE	257
LDPE/PCH-BTB (10:1)	225
LDPE/PCH-BTB (30:1)	230

5. CONCLUSION

Porous clay heterostructure (PCH) is a porous material that can be prepared by the polymerization of tetraethoxysilane (TEOS) in the presence of surfactant micelles within the galleries of bentonite. The functionalized PCH with amino group which was named APPCH can be prepared by co-condensation reaction in the galleries of bentonite. Chromophores, bromothymol blue and methyl red were added to the PCH and APPCH respectively to obtain the colorimetric properties for smart films. To confirm the formation of porous structure, the products were characterized by N_2 adsorption-desorption, XRD, SEM and FTIR techniques. The results revealed that PCH had the high surface areas of 524.1 m^2/g, average pore diameter of 4.85 nm and pore volume of 0.64 cc/g while the functionalized PCH (APPCH) had the less surface area and pore volume in the range of 119.8-320.5 m^2/g and 0.33-0.42 cc/g, respectively. The rugged surface of SEM image and no sharp peaks from XRD spectra was used to confirm the porous structure in APPCH and PCH. In addition, surface area and pore volume of APPCH and PCH decreased after modified with pH-dye indicated that the incorporation of pH dye in APPCH and PCH was successful. A color indicator for detecting fish and climacteric fruit freshness was developed based on PP/APPCH-MR nanocomposite films and LDPE/PCH-BTB nanocomposite films respectively. The results showed that the increase of total volatile basic nitrogen (TVB-N) values from 0-8 hours corresponded to the color change of indicator films from red to light orange during fish spoilage. The color change of indicator films from green to yellow correlated with standard CO_2 levels, which can be compared to CO_2 levels from respiration during fruit ripening. These pH indicator films could be used to determine fish freshness and can be applied for detecting the quality of climacteric fruit by color change. The both nanocomposites showed the higher thermal stability due to the presence of porous clay in nanocomposite. Moreover, both nanocomposite showed the improvement in oxygen barrier properties.

6. RECOMMENDATIONS

Based on what we have been discovered in this study, the following recommendations are suggested in following scopes.

(1) Study on the use of other indicator type in order to develop smart packaging to be more effective.

(2) Study at low/refrigerated temperature

(3) Study on the use of indicator film for the other types of climacteric fruits such as mango and durian.

7. REFERENCES

Ahivenainen, R. and Smolander, M. (2003). The Use of Freshness Indicators in Packaging. Novel Food Packaging Techniques, 127-143. Cambridge England: Woodhead Publishing Limited.

Araki, S., Doi, H., Sano Y., Tanaka, S. and Miyake Y. (2009). Preparation and CO_2 Adsorption Properties of Aminopropyl-Funtionalized Mesoporous Silica Microspheres. Journal of Colloid and Interface Science, 339, 382-389.

Baixas-nogueras, S., Bover-cid, S., Veciana-nogués, T. and Vidal-carou, M. (2002). Chemical and Sensory Changes in Mediterranean Hake (Merluccius merluccius) under Refrigeration (6-8 °C) and Stored in Ice. Journal of Agricultural and Food Chemistry, 50, 6504-6510.

Choy, J. H., Kwak, S.Y., Han, Y. S. and Kim, B. W. (1997). New Organo-Montmorillonite Complexes with Hydrophobic and Hydrophilic Functions. Materials Letters, 33, 143-147.

Ding, C., Jia, D., He H., Guo, B. and Hong, H. (2005). How Organo-Montmorillonite Truly Affects the Structure and Properties of Polypropylene. Polymer Testing, 24, 94-100.

Gane, R. (1936). A Study of the Respiration of Banana. Ph.D. Research, Cambridge, United Kingdom.

Gram, L. and Huss H. (1996). Microbiological Spoilage of Fish and Fish Products. International Journal of Food Microbiology, 33, 121-137.

Hong, S. and Park, W. (2000). Use of Color Indicators as an Active Packaging System for Evaluating Kimchi Fermentation. Journal of Food Engineering, 46, 67-72.

Mattayan, A., Manuspiya, H. and Magaraphan, R. (2009). Induced Magnetic Properties to Surface Modified Mesoporous Porous Clay Heterostructures for Sensor Application in Food Packaging. M.S. Thesis, The Petroleum and Petrochemical Collage, Chulalongkorn University, Bangkok, Thailand.

Modesti, M., Lorenzetti, A., Bon, D. and Besco, S. (2006). Thermal Behavior of Compatibilised Polypropylene Nanocomposite: Effect of Processing Conditions. Polymer Degradation and Stability, 91, 672-680.

Nakatsuji, M., Ishii, R., Wang, Z. M. and Ooi K. (2004). Preparation of Porous Clay Minerals with Organic–Inorganic Hybrid Pillars Using Solvent-Extraction Route. Journal of Colloid and Interface Science, 272, 158-166.

Nopwinyuwong, A., Trevanich, S. and Suppakul, P. (2010). Development of a Novel Colorimetric Indicator Label for Monitoring Freshness of Intermediate-Moisture Dessert Spoilage. Talanta, 81, 1126-1132.

Pacquit, A., Lau, K., McLaughlin, H., Frisby, J., Quilty, B. and Daimond, D. (2006). Development of a Volatile Amine Sensor for the Monitoring of Fish Spoilage. Talanta, 69, 515-520.

Pacquit, A., Frisby, J., Daimond, D., Lau, K., Farrel, A., Quilty, B. and Daimond, D. (2007). Development of a Smart Packaging for the Monitoring of Fish Spoilage. Food Chemistry, 102, 466-470.

Pavlidou, S. and Papaspyrides, C. (2008). A Review on Polymer–Layered Silicate Nanocomposites. Progress in Polymer Science, 33, 1119-1198.

Santamaria, P. and Eguiazabal, J. I. (2012). Structure and Mechanical Properties of Blown Films of Ionomer-compatibilizerd LDPE Nanocomposites. Polymer Testing, 31, 367-374.

Seephueng, A., Manuspiya, H. and Magaraphan, R. (2008). Smart Packaginfg for Fish Spoilage Indicator. M.S. Thesis, The Petroleum and Petrochemical Collage, Chulalongkorn University, Bangkok, Thailand.

Srithammaraj, K., Manuspiya, H. and Magaraphan, R. (2011). Modified Porous Clay Heterostructures by Organic–Inorganic Hybrids for Nanocomposite Ethylene Scavenging/Sensor Packaging Film. Packaging Technologies and Science.

Tassanawat, S., Manuspiya, H., Magaraphan, R. and Nithithanakul, R. (2007). Polypropylene/Organoclay Nanocomposite for pH-sensitive Packaging. M.S. Thesis, The Petroleum and Petrochemical Collage, Chulalongkorn University, Bangkok, Thailand.

Wei, L., Tang, T. and Huang, B. (2004). Novel Acidic Porous Clay Heterostructure with Highly Ordered Organic-Inorganic Hybrid Structure: One-Pot Synthesis of Mesoporous Organosilica in the Galleries of Clay. Microporous and Mesoporous Materials, 67, 175-179.

Wu, Z., Xiang, H., Kim, T., Chun, M. S. and Lee K. (2006). Surface Properties of Submicrometer Silica Spheres Modified with Aminopropyltriethoxysilane and Phenyltriethoxysilane. Journal of Colloid and Interface Science, 304, 119-124.

Yam, K., Takhistov, P. and Miltz, J. (2005). Intelligent Packaging: Concepts and Applications. Journal of Food Scienc, 70.